ISTANBUL TECHNICAL UNIVERSITY ★ GRADUATE SCHOOL OF SCIENCE ENGINEERING AND TECHNOLOGY

OPTIMUM DESIGN OF ATTENUATOR OF SPUN-BOND PRODUCTION SYSTEM

M.Sc. THESIS

Nasser GHASSEMBAGLOU

Department of Mechanical Engineering

Mechanical Design Programme

July 2015

ISTANBUL TECHNICAL UNIVERSITY ★ GRADUATE SCHOOL OF SCIENCE ENGINEERING AND TECHNOLOGY

OPTIMUM DESIGN OF ATTENUATOR OF SPUN-BOND PRODUCTION SYSTEM

M.Sc. THESIS

Nasser GHASSEMBAGLOU
503121218

Department of Mechanical Engineering

Mechanical Design Programme

Thesis Advisor: Prof. Dr. Hikmet KOCABAŞ

July 2015

İSTANBUL TEKNİK ÜNİVERSİTESİ ★ FEN BİLİMLERİ ENSTİTÜSÜ

Spunbond-Nanolif-Spunbond (SNS) Teknolojisi İle Nitelikli Hava Filtresi Üreten Bir Sistemin Çekici Ünitesinin Tasarımı ve Geliştirilmesi

YÜKSEK LİSANS TEZİ

Nasser GHASSEMBAGLOU
503121218

Makina Mühendisliği Anabilim Dalı

Konstrüksiyon Programı

Tez Danışmanı: Prof. Dr. Hikmet Kocabaş

Temmuz 2015

Nasser Ghassembaglou, a **M.Sc** student of ITU **Graduate School of Mechanical Engineering** student ID **503121218**, successfully defended the **thesis** entitled "Optimum Design of Attenuator of Spun-bond Production System", which he prepared after fulfilling the requirements specified in the associated legislations, before the jury whose signatures are below.

Thesis Advisor : **Prof. Dr. Hikmet KOCABAŞ**
Istanbul Technical University

Jury Members : **Prof. Dr. Şafak YILMAZ**
Istanbul Technical University

Doç. Dr. Oktay YILMAZ
Yıldız Technical University

Date of Submission : 09 July 2015
Date of Defense : 02 July 2015

To my family specially my mother and be loved father,

FOREWORD

This thesis has been prepared under the supervision of Prof. Dr. Hikmet Kocabaş; it was not possible to be succeeded in this work without his support and guidance. I hereby give my best thanks to him who didn't withhold any support, effort and understanding at this project.

I appreciate the precious contribution of Prof. Dr. Şafak Yılmaz, Assist. Prof. Ertan Öznergiz and Assist. Prof. Oktay Yılmaz. There was an enormous amount of work which I wasn't able to do without their help and support.

During this work I confronted so many hardships and problems, which were not possible to be conquered without the mental support of my family, especially my mother. I am very thankful to them and feel gratitude toward their support.

I gratefully acknowledge the financial support of The Scientific and Technological Research Council of Turkey (TÜBİTAK) and Scientific Research Projects (BAP) Institution, through grant number: 112M311.

July 2015 Nasser Ghassembaglou

TABLE OF CONTENTS

Page

ABBREVIATIONS

CFD **:** Computational Fluid Dynamics
SNS **:** Spunbond-Nanofiber-Spunbond

LIST OF TABLES

Page

LIST OF FIGURES

Page

OPTIMUM DESIGN OF ATTENUATOR OF SPUN-BOND PRODUCTION SYSTEM

SUMMARY

Nanofibers are effective materials, which have frequently been investigated to produce high quality air filters. As an environmental approach, our aim is to achieve nanofibers by melting. In spun-bond systems extruder, spin-pump, nozzle package and attenuator are used. Molten polymer which flows from extruder is made steady by spin-pump. Regular melt passes through nozzle holes and forms fibers under high pressure. The fibers pulled from nozzle are shrunk to micron size by an attenuator; after solidification, they are collected on a conveyor. In this research, different designs of attenuator systems have been studied; also CFD analysis have been done on these different designs. Afterwards, one of these designs tested and finally some optimizations have been done to reduce pressure drop and increase air velocity.

As a nanofiber production method, electrospinning has intensively been investigated recently. However, lots of solvent are used in traditional electrospinning method which reduces production rate. Moreover, this method increases production costs. Therefore, melting system was invented as a basic method for SNS nanofiber layer fabrics production. In this system, extruder, nozzle package and high-voltage power supply are essential devices. Mixture or molten polymer is put in a funner which has one or more holes. In this process polymer granules are fed by funner which are melted and moved on by extruder. After extruder, granules are driven to a nozzle which has numerous holes and are converted to fibers. Coat- Hanger die has been designed and selected to be used in this research. Its primitive representation has been designed by an analytical method.

After nozzle, molten polymer is solidified by cold air. In attenuation region fibers are attenuated by high speed air. Depending on the polymer characteristics and production rate, air velocity reaches 1000 to 8000 m/min. For instance, polypropylene (PP) usually needs a 2000 m/min velocity where this amount is about 4000 m/min for polyamide (PA). Through cooling and protracting process, parameters such as humidity and temperature should be controlled.

Fibers diameter and its homogeneity are two main factors which determine performance of produced filter. In order to achieve this goal polymer pressure in the nozzle and also air pressure distribution at jet section must be uniform.

By inspecting so many different references and patents, a primitive design for attenuator has been developed. The design had to be done at a state which guaranties high velocity with lowest vibration. Vibration is an important factor in attenuator design; it results in agglomerated nanofibers and subsequently non-uniformity. A primitive design of attenuator has been created and some analysys have been done to probe velocity and pressure drop in it. Selected design has been drawn and meshed in ANSYS-ICEM CFD. The mesh method which has been used in this process is a very accurate one which uses blocks instead of automatic meshing.

Selected design has been manufactured and a fan with 0.07 bar output pressure has been purchased in the sake of experiments. Manufactured attenuator has been mounted on the fan and jet velocity tests have been done on it.
There was a very close overlapping between experimental and simulation results where max deviation is 8%. Therefore, some optimizations could be done based on simulation results.
However, sometimes there would be needs for higher velocities which would requests fans with higher output pressure and subsequently higher powers. In this situation, demanded fan will be very large and expensive. Moreover, less pressure drop will guarantee less vibration. So it is needed to obtain higher velocities with lower pressure drop by doing some optimizations on attenuator interior design which affects pressure drop significantly.

Therefore, some researches has been done on this matter and a new interior design has been developed. This process should be done on a layout which guarantees smooth narrowing throughout air path; so the least possible amount of pressure drop will be obtained. In this process, to reduce pressure drop, a larger input has been selected which is as large as fan output. As mentioned before, there was a large amount of pressure drop at the wall next to inlet pipe; this pressure drop was the product of high velocity in the pipe which was a result of small diameter; this problem was conquered by enlarging inlet gap. Moreover, there was a significant pressure drop at the pipe itself which was very long; to eliminate this, the pipe removed from representation. Also interior design has been made in a case which has a smooth narrowing layout. At first, some air channels with a slight angle have represented; these angles would provide a perfect narrowing at channels; but as a matter of fact, it was very difficult to manufacture such channels; so the angles have been eliminated and some other methods employed to compensate the lack of inclined designed. Air partitions have been made vertical and by using longer partitions in every path, smooth narrowing made possible. There was a significant pressure drop because of sharp exit on jet; severe colliding of air to the plate next to jet had caused in mentioned pressure drop; so it has been changed to a 45 degrees exit on bottom edge of jet gap. In order of comparisons, a simulation with the same properties of former one has been done on this layout. This will guarantee an accurate comparison between two designs, which will lead to a realistic conclusion.

By using same inlet properties, there was a 60 m/s growth in jet velocity which is about 90 m/s. In addition, pressure drop at the wall next to inlet and jet have been eliminated. There was a large amount of pressure drop at interior part of attenuator unit which have been reduced significantly by changing some design parameters. Also by using the same properties of inlet a three times larger amount of velocity has been obtained at jet section which will help to protract nanofibers more than before. Also by using smooth narrowing method at interior part there will be less vibration which will help to obtain more uniform spun-bonds.
Finally, in order to find out the effect of fibers on airflow, other CFD analysis have been done considering fibers at cross sections. There are 396 exit holes on manufactured die with a diameter of 0.35 mm which brought some hardships during meshing process. This geometry has been meshed using advanced method of structured mesh and analyzed in FLUENT. Results of these analysis shows a slight effect of fibers on airflow, which is not so great to consider in attenuator design.
A UDF code has been developed during this project to consider fibers movements between two attenuator units; the method which is used in this analysis is deforming

mesh which is brought in FLUENT. However, this analysis would need a computer with very high ram capacity and a great CPU; so because of lack of computational resources, it wasn’t possible to do such an analysis.

It is obvious that changing a design representation slightly could have a significant effect on pressure drop and production factors. In this way, the most important part in this project was drawer unit. Slight changes at interior or exterior parts of drawers would has a significant effect on pressure drop. It is necessary to consider the cost of production at first steps, which includes fan as an expensive component. Using analytical methods could help to prevent large amount of financial wastes, if it is done using a true and useful method.

SPUNBOND-NANOLİF-SPUNBOND (SNS) TEKNOLOJİSİ İLE NİTELİKLİ HAVA FİLTRESİ ÜRETEN BİR SİSTEMİN ÇEKİCİ ÜNİTESİNİN TASARIMI VE GELİŞTİRİLMESİ

ÖZET

Nanolifler, yüksek nitelikli hava filtresi üretmek için son dönemde sıklıkla araştırılan etkili malzemelerdendir. Bu tezdeki SNS yapı spunbond ve nanoağ katmanlarından oluşmaktadır. Nanoağ filtre malzemesinin niteliğini belirlemektedir. Lif çapı nano boyuttadır. Bu yüzden üretilen kumaşın gözenek çapı düşüktür. Bu sayede mikron boyutundan küçük parçacıkları tutabilecek kadar niteliklidir. Nanoağ ile üretilen kumaşın dayanımı çok düşüktür. Hemen dağılmaktadır. Filtrenin dayanımını artırmak için nanoağ katmanının iki tarafı spunbond yöntemiyle üretilen kumaşla kaplanılacaktır. Bu sayede spunbond- nanolif-spunbond (SNS) katmanları ile yüksek nitelikli hava filtresi üretilmiş olacaktır. Spunbond katmanı mikron boyutunda lif çapına sahiptir ve filtre kağıdının dayanımını artırmak için kullanılacaktır.

Spunbond katmanında karşılaşılan sorun ise kumaşın kalınlığının homojen olmamasıdır. Bölgesel olarak kalınlığın değiştiği görülmektedir.

SNS, yani spunbond-nanolif-spunbond şeklinde sandviç bir yapı düşünülmekte, bu sayede nanoliflerin düşük mekanik özelliklerinin filtrasyon şartlarına ayarlanması planlanmaktadır. Spunbond yöntemi ile üretilecek olan 5-30 mikron boyutunda lif çapına sahip olan katman filtrenin dayanımını artıracak olan katmandır. Nanolif katmanı ise filtrenin performansını, gözenekliliğini belirleyen katmandır. Bu katmanda lif çapı nano boyuttadır ve bu yüzden nanolifdeki gözenekler spunbonda göre daha küçüktür. Çevresel bir yaklaşım olarak eriyikten nanolif eldesi hedeflenmektedir. Oldukça yenilikçi bir çalışma olmasından bu tip malzemelerin üretimini sağlayacak spunbond ve nanolif üretim teknolojilerine yönelik makina tasarımı eksenlidir

Spunbond yönteminde kullanılacak sistem ekstrüder, spinpump, düze paketi, sıcak ve soğuk hava kabinlerinden oluşacaktır. Spunbond yönteminde ekstrüderden eriyik halde çıkan polimerin spinpump ile akışı düzenli hale getirilmektedir. Düzenli akan eriyik yüksek basınç altında düze paketindeki deliklerden geçerek lif haline getirilmektedir. Düzeden çıkan lifler önce sıcak hava kabini, sonra da soğuk hava kabini ile çekilerek mikron boyutuna düşürülmekte ve katılaşarak konveyör üzerinde toplanmaktadır. Oluşan liflerin aynı çapta olması ve üretilecek olan kumaşta lif dağılımının homojenitesi filtre performansını belirten iki ana faktördür. Bunu sağlayabilmek için düzede polimer basınç ve çekim bölümünde hava basınç dağılımının eşit olması gerekmektedir. Bu iki problem spunbond mamul kalitesinde ana etkendir ve yüksek derecede reoloji ve imalat mühendisliği birikimi gerektirmektedir.

Hava çekim ünitesi eksenel olarak iki ayrık alt üniteden oluşmaktadır. Bu alt ünitelerin tasarımı ve aynı zamanda gerekli analizleri bu tezde araştırılmış ve sonuçlar deneysel olarak onaylanmıştır. Son olarak tez kapsamında en iyi tasarım çözümü araştırılıp ilgili analizleri yapılmıştır.

İlk başta projede kullanma amacıyla bir düze paketi seçilmiştir. Düze paketi 396 tane 0.35 milimetre deliğe sahiptir; malzeme ekstrüder ve düze paketinde eriyik hale geldikten sonra spinpump yardımı ile bu deliklerden dışarıya akar ve bir çekici ünitesinden geçerek uzamak ile birlikte incelir. Bu işlemde kullanılan çekici ünitesi için, ilk başta bir ön tasarım düşünülmüş ve üzerinde Hesaplamalı Akış Analizleri (HAD) yapılmıştır. Analiz sonuçlarına dayanarak bir tasarım yapılmış ve onun üzerinde analizler gerçekleşmiştir. Analizlerde elde edilen sonuçları doğrulamak üzere bu çekici imal edilmiş ve üzerinde hız denemeleri yapılmıştır. Düşük maliyete sebep olsun diye mevcut olan bir fandan yardım alınmıştır. Ama bu fanın çıkış değerleri istenilen değerlerden düşük olduğundan, fanın çıkış değerleri ile yeni analizler yapılmış ve sonuçlar kıyaslanmıştır. Deneme ve analiz sonuçların yakın bir şekilde ve 8% hata ile örtüşmesi yeni tasarımlarda HAD analizleri sonuçlarına güvenime yol açmıştır.

Deneme fanı boyutlarına ve elde edilen hızlara bakıldığında, mevcut tasarım için lazım olan fanın çok büyük boyutlarda olacağı tespit edilmiştir. Aynı zamanda denemelerde bazı sorunlar ile karşılaşılmıştır.

Bu sorunları giderme ve basınç kaybını düşürme amacı ile yeni bir tasarım düşünülmüştür. Yeni tasarımda basınç kaybını düşürmek için çekicinin iç tasarımı ve jet kısmında bazı değişiklikler yapılmasına karar verilmiştir. Hava bölmeleri kısmında daha düşük basınç kaybına uğramak için, bu bölmeler dikey hale getirilmiş ve uzatılmıştır. Havanın dar bir bölgeden daha geniş bir bölgeye girmesi basınç kaybına neden olmaktadır. Bu problemi çözmek için hava bölmelerinin açılı ve daralarak yapılmasına karar verilmiştir. Analizlerde bu işlemin çok yararlı olduğu gözlemlenmiştir; ama imalat problemleri nedeni ile bu bölmelerin açısız yapılmasına gerek duyulmuştur. Aynı koşullarda başka analizler açısız bölmeler ile yapılmış ve yüksek bir etkisi olmadığı gözlemlenmiştir.

Hava girişinin karşı duvarında havanın yüksek hızla çarpması nedeni ile büyük basınç kayıpları gözüküyor. Aynı zamanda havanın fanın çıkışından çekici girdiğinde basınç kaybına uğramamasına özen göstermek gerekiyor. Bu iki problemi çözmek için, yeni tasarımda, hava girişi daha büyük çaplı ve dört gen olarak seçilmiş. Analizler yapılan değişikliğin girişin karşı duvarında ve giriş borusunda olan basınç kaybını tamamen yok ettiğini göstermektedir.

Jet bölümünde havanın yüksek hız ile jetin plakasına çarptığı için yüksek basınç kaybı gözlemleniyor. Bu problemi gidermek için jet çıkışını 90 derece açılı yerine 45 derece açıyla yapılmasına karar verilmiştir. Yine bu tasarımın üzerinde analizler yapılmış ve doğru etkisi onaylanmıştır.

Denemelerde görüldüğü gibi havanı yüksek hız ile jetin karşı duvarına çarptığında, onun eğilmesine ve sonuç olarak hazın düşmesine neden olduğu anlaşılmıştır. İlk tasarım imalatında malzeme olarak alüminyum kullanılmıştı. Eğilme problemini çözmek için yeni tasarımda paslanmaz çelik kullanımına karar verilmiştir.

Alüminyum ile imalat yapımında, alüminyum kaynağının zor bir işlem olduğundan ve aynı zamanda kaynağın alüminyumun deforme olmasına yol açtığından, bu malzemenin değiştirilmesi öne sürülmüştür. Bu amaçla ve bir önceki problemin çözümü doğrultusunda yeni tasarımın paslanmaz çelikten yapılmasına karar verilmiştir. Paslanmaz çeliğin kullanımı imalat aşamasında hızlanmaya da sebep olacaktır.

Yapılan tüm deliklikLerden sonra yeni tasarım üzerinde HAD analizleri yapılmış ve bir önceki sonuçlar ile kıyaslanmıştır. Bu analizler deneyim fanının çıkış değerleri ile yapılmıştır. Analizlerin sonucunda jet bölümünde hava hazının 60 m/s kadar yükseldiği ve başka bir değişle 90 m/s saniyeye ulaştığı gözlemlenmiştir.

Son olarak liflerin hava akışı üzerinde etkisini görme amacı ile yeni analizler lifler ile birlikte yapılmış ve sonuçlar incelenmiştir. Bu analizler liflerin hava akışı ve hızı üzerinde fazla bir etkisi olmadığını göstermiştir.

Aynı zamanda liflerin hareketini de göz önünde bulundurmak için bir UDF (User Defined Fucntions) hazırlanmıştır. Bu UDF de kullanılan modül, “deforming mesh”tir. Bu koşturuyu yapmak için büyük belleğe sahip bilgisayarlara ihtiyaç duyulmaktadır. Bu olanakların eksik olduğundan bu analizi yapmak mümkün olmamıştır.

Çekicinin iç tasarımında en küçük değişikliklerin basınç kaybını büyük ölçeklerde etkilediği gözlemlenmiştir. İmalat ve eleman maliyetlerini ilk başta düşünülmesi büyük bir önem taşımaktadır. Bu işlemde yüksek kapasiteli bir fan en fazla ağırlığı taşımaktadır. HAD analizleri doğru kullanıldığında mali olanakların yanlış yönde harcanması ve zaman tasarrufuna neden olacaktır.

1. INTRODUCTION

Spun-bond Method is a prevail one in nonwoven fabrics production. Its fabrics are formed by laying fibered molten polymer on a conveyor. Fibers are spread by electrostatic loads or air jet at drawing stage. Gathering surface is generally perforated to prevent fibers diversion and uncontrolled conveyance. In this process polymer granules are feed by feeder. These granules are melted and pushed forward by using an extruder. Afterwards, they are fibered by a perforated die and lied on a narrow tape, which ends up on hot cylinders to get fastened. Finally, wrapping process is done on taken fibers. Different materials such as polypropylene, polyester, nylon, polyethylene, polyurethane, and synthetic silk are used in this process [1].

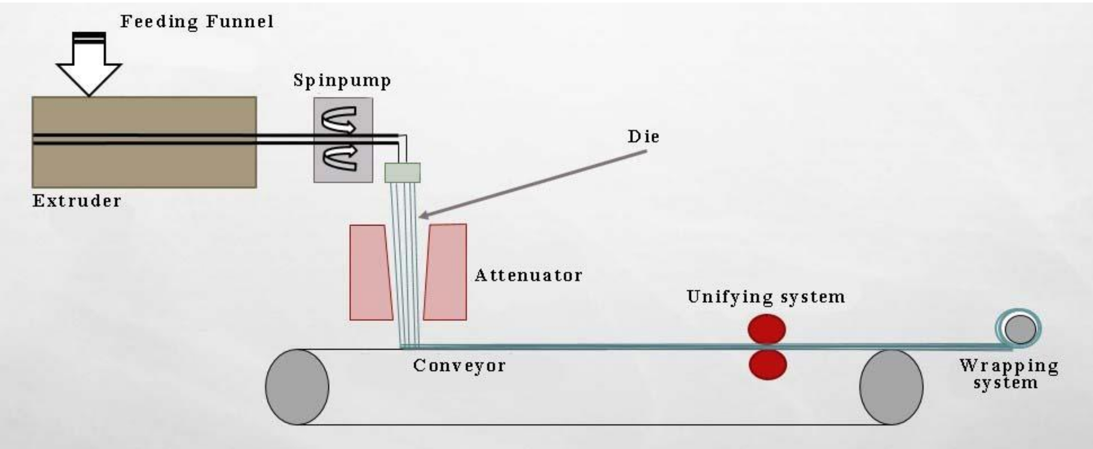

Figure 1.1 : Spun-bond Method.

Equipment which are used in Spun-bond method and also flow scheme are shown in Figure 1.2.

1.1 Literature Review

1.1.1 Pneumatic fiber drawing systems

There are three different systems which are generally encompasses all systems in spun-bond method [1]. These are Docan (Figure 1.3 a), Reicofil (Figure 1.3 b), and Lutravil (Figure 1.3 c) systems.

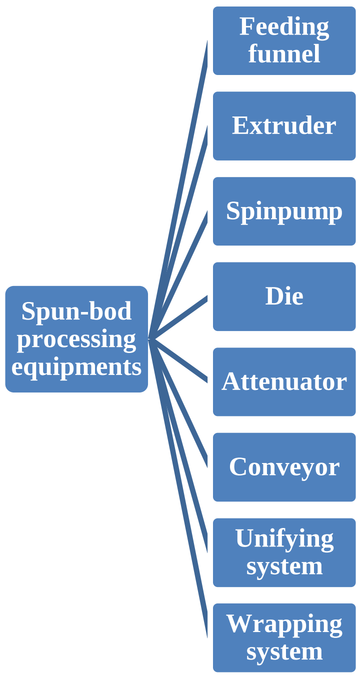

Figure 1.2 : Equipment used in Spun-bond method.

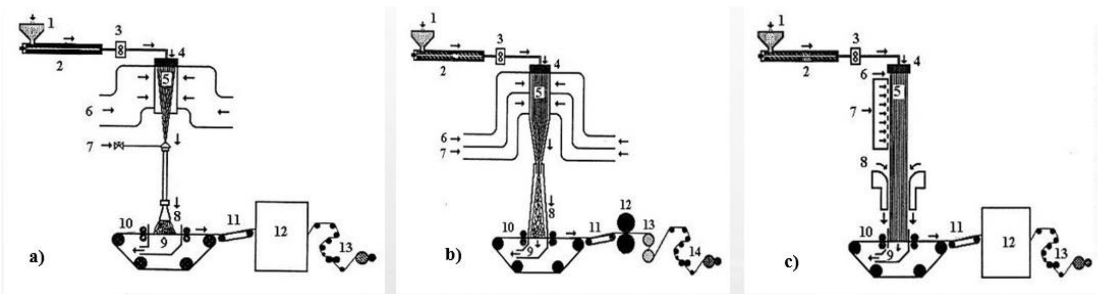

Figure 1.3 : a) Docan System, b) Reicofil System, and c) Lutravil System.

In Docan system, another air stream named operational air are used after cold air blower to draw fibers uniformly. Afterward, drawing and laying processes and right after unification and wrapping operations are done on fibers [1].

In the case of Reicofil system, there is a second air blower helping the main cold air stream. Afterwards, there is a fiber mixing system. Again fibers are unified by hot spools in a different method and right after cooling roll is used [1].

There are three different air systems in Lutravil method. Also, there is a different unifyıng system in comparison with Docan and Reicofil methods.

Spun-bond fabrics show properties which are between woven fabrics and paper specifications. It’s possible to produce spun-bond fabrics which are light and elastic or heavy and hard [2].

To obtain very thin fibers, molten polymer is passed into a high speed air corridor. Generally there are four different types of pneumatic fiber drawing systems in spun-bond production. These are Docan, Reicofil, Lutravil [3], and Fumin Lu- Ason [4]. Every drawing (thinning) system has similar parts: cooling, drawing with high speed air and a diversion system right before the conveyor. At first, polymer is cooled with an air stream of 10- 15^{oC} in temperature and 1- 2 m/s in speed. Then, relatively thick and solidified fibers are entered into pneumatic drawing system. As shown in Figure 1.4, air jet is located near air corridor entrance. Air velocity can excess sound's speed from time to time (Figure 1.5). While air has a laminar flow at mold exit, it has a turbulence characteristics at pneumatic drawing area.

High speed air is generally provided by a compressor; but it can sometimes be replaced by a powerful fan. The pressure of compressor could be between 5 and 50 bar. High speed air applies dragging force to polymer fibers. Fibers which are in molten at mold exit, are made thinner by dragging force. In commercial production pneumatic system air velocity is between 6000- 18000 m/min (100- 300 m/s) and fibers drawing speed is between 1000- 6000 m/min (17- 100 m/s). There are always differences between air and fibers speed. In this process air velocity is 2 or three times more than fibers drawing speed. In order to prevent mixing and combination of fibers at air corridor, turbulence shouldn't be too much at this section. As a result, there are a variety of designs in patents. By considering this, air jet is designed parallel with fibers itinerary. There are different designs too. In those systems there isn't any air jet. Instead of it, cooling air, which is used at exit section of die, is exploited to draw fibers by reducing air cross section that results in speed increment. The least turbulence is obtained by using this design.

Reicofil spun-bond system is a closed one from die to conveyor which is mostly used in commercial production. Fiber dissipation is a mandatory part to obtain an irregular network (felt). This part is generally designed by two different method. Figure 1.6 shows first design; as shown in this figure, air corridor has a widening design by advancing to its exit. This condition results in a back pressure which reduces air velocity and drawing force acting on fibers simultaneously. There is a slight distance between pneumatic drawer and conveyor at second design. When fibers get out of pneumatic drawing unit, effective drawing tension suddenly drops to zero. At this situation, fibers are drew back and fringed. These two systems are sometimes merged, where widening through the exit of pneumatic unit is exploited as well as setting an appropriate distance between this unit and conveyor.

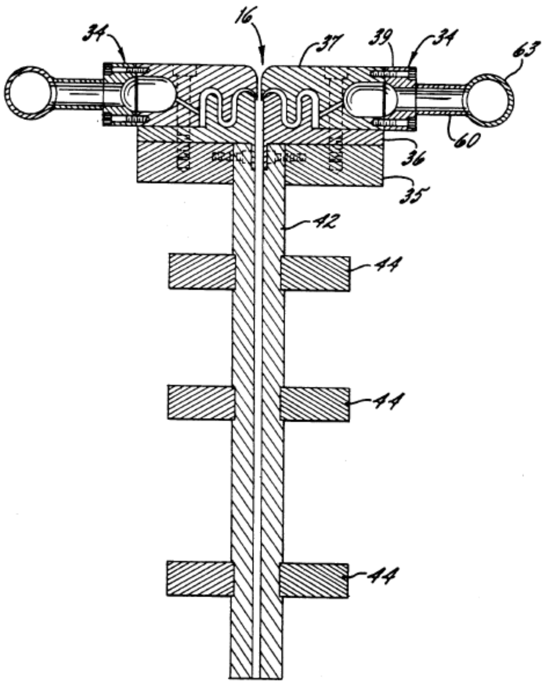

Figure 1.4 : A typical pneumatic fiber drawing system [5].

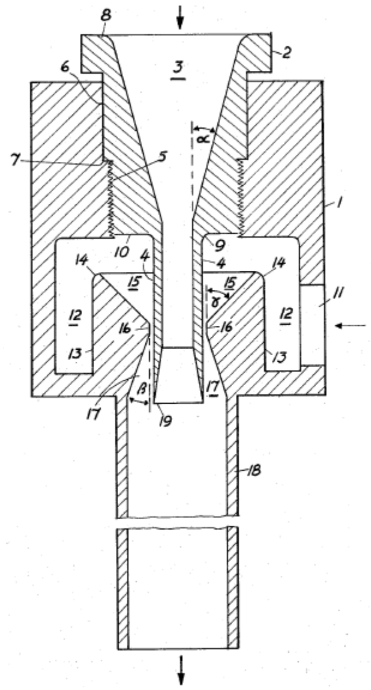

Figure 1.5 : A special design of air jet [6].

Docan, Lutravil (Figure 1.7) and Fumin Lu-Ason suggest separate cooling and fiber drawing systems. Pneumatic drawing unit is placed between conveyor and die. In order to prevent adherence between fibers themselves and also fibers and drawing system surfaces, fibers should be solidified at drawing unit entrance. As a result of this, fibers are cooled at cooling section by forced flow. To obtain these, the distance between drawing unit and die should be optimized to its best. There is no need to cooling system in some applications. At the other hand, in Fumin Lu-Ason spun-bond system [7], it’s needed to guide fibers into pneumatic fiber drawing unit while they are molten; while the distance between drawer and die is 1 to 3 m in other spun-bond methods, this distance reduces to 20 to 90 cm between die and drawer in this system. In this condition, as a result of higher temperature and shorter fiber to draw, prolongation viscosity is less; so fibers are slenderized more by equal drawing force. Thinner fibers are cooled sooner; and as a result of tension, which cause crystallization, are solidified at higher temperatures. As shown in Figure 1.8, air jet is guided to polymer fibers at a certain angle. This organization is set to intense turbulence which will produce more entwined fiber textile. The maximum speed of fibers is obtained by exploiting this system [8]. Altitude of conveyor and drawing unit is adjustable in Fumin Lu-Ason method.

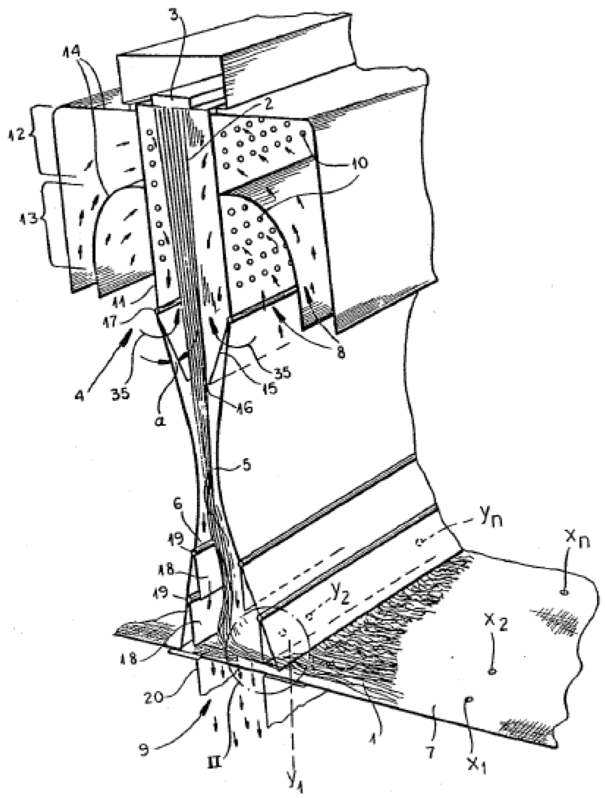

Figure 1.6 : Reicofil spun-bond system.

To produce stable nonwoven fabrics, system should start in low operating parameters (low molten polymer flux, low air velocity and large distance between die and drawer). Through production levels of operation parameters are increased and distance between die and drawer unit is reduced.

Here are some general parameters of spun-bond process system:

Molten polymer: 0.5-4 g/hole/min

Molten polymer temperature for polypropylene: 210-320 ^oC

Final fiber diameter in nonwoven fabrics: 1-50 µm

To reduce final diameter of fibers it is mandatory to increase drawing speed by higher air velocity, decrease molten viscosity by increasing temperature of molten polymer and air at the exit section of die and finally decrease molten polymer flow rate.

Thesis encompasses a design similar to Lutravil pneumatic fiber drawing system shown in Figure 1.7.

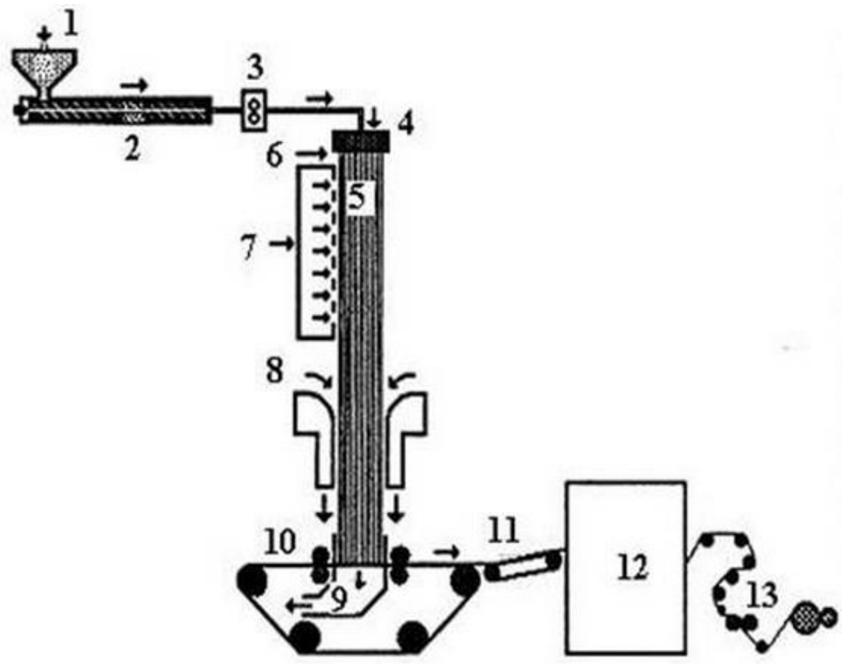

Figure 1.7 : Lutravil spun-bond system [3].

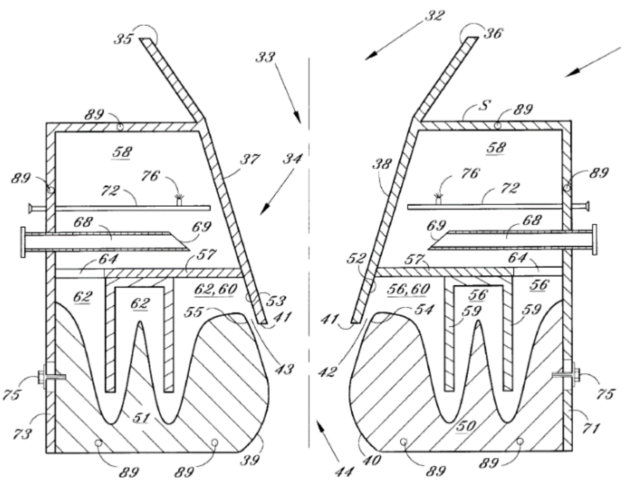

Figure 1.8 : Fumin Lu-Ason system and its pneumatic fiber drawing unit [7].

1.1.2 Strategy of Computational Fluid Dynamics (CFD)

To assume air velocity and pressure drop in attenuator, some CFD analysis have been used primitively.

1.1.2.1 Strategy of Computational Fluid Dynamics (CFD)

Broadly, the strategy of CFD is to replace the continuous problem domain with a discrete domain using a chosen mesh or grid. In the continuous domain, each flow variable is defined at every point in the domain. For instance, the pressure p in the continuous 1D domain shown in Figure 1.9 would be given as

$$p = p(x), 0 < x < 1 \quad \textbf{(1.1)}$$

Continuous Domain $0 \leq x \leq 1$

Figure 1.9 : Coupled PDEs + Boundary conditions in continuous variables [9].

In the discrete domain, each flow variable is defined only at the grid points. So, in the discrete domain shown in Figure 1.10, the pressure would be defined only at the N grid points.

$$p_i = p(x_i), i = 1, 2, \ldots, N \quad \textbf{(1.2)}$$

Discrete Domain $x = x_1, x_2, \ldots, x_N$

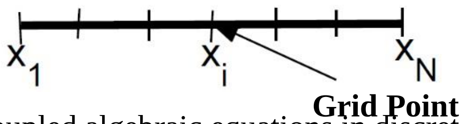

Figure 1.10 : Coupled algebraic equations in discrete variables [9].

In a CFD solution, one would directly solve for the relevant flow variables only at the grid points. The values at other locations are determined by interpolating the values at the grid points.

The governing partial differential equations and boundary conditions are defined in terms of the continuous variables p (pressure) and $\vec{V}$ (Velocity) etc. One can approximate these in the discrete domain in terms of the discrete variables p_i, V_i, etc. The discrete system is a large set of coupled, algebraic equations in the discrete variables. Setting up the discrete system and solving it (which is a matrix inversion problem) involves a very large number of repetitive calculations.

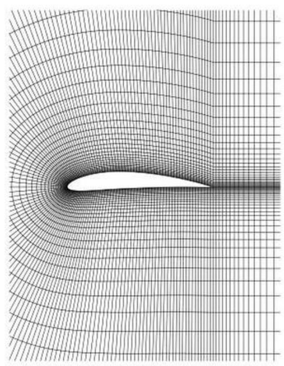

Figure 1.11 : Grid used for solving the flow over an airfoil [9].

1.1.2.2 Discretization using the finite-difference method

To keep the details simple, consider a simple 1D equation:

$$\frac{du}{dx} + u = 0\,; 0 \leq x \leq 1\,;\ u(0) = 0 \qquad \textbf{(1.3)}$$

A discrete representation of Equation **(1.3)** will be derived on the following grid:

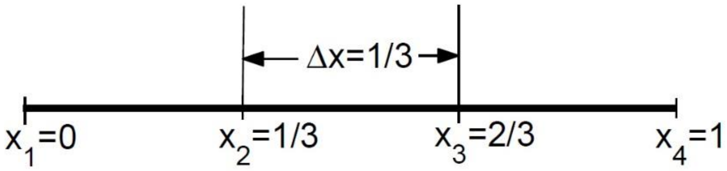

Figure 1.12 : Calculation field [9].

This grid has four equally-spaced grid points with Δx being the spacing between successive points.

Since the governing equation is valid at any grid point,

$$(\frac{du}{dx})_i + u_i = 0 \qquad \textbf{(1.4)}$$

where the subscript *i* represents the value at grid point x_i. In order to get an expression for $(\frac{du}{dx})_i$ in terms of u at the grid points, u_{i-1} is expanded in a Taylor's series

$$u_{i-1} = u_i - \Delta x \left(\frac{du}{dx}\right)_i + O(\Delta x^2) \qquad \textbf{(1.5)}$$

Rearranging gives

$$(\frac{du}{dx})_i = \frac{u_i - u_{i-1}}{\Delta x} + O(\Delta x) \qquad \textbf{(1.6)}$$

The error in $(\frac{du}{dx})_i$ due to the neglected terms in the Taylor's series is called the truncation error. Since the truncation error above is $O(\Delta x)$, this discrete representation is termed first-order accurate.

Using Equation **(1.6)** in Equation **(1.4)** and excluding higher-order terms in the Taylor's series, the following discrete equation is gotten:

$$\frac{u_i - u_{i-1}}{\Delta x} + u_i = 0 \qquad \textbf{(1.7)}$$

Here an algebraic equation has been derived from a differential equation.
This method of deriving the discrete equation using Taylor's series expansions is called the finite-difference method. However, most commercial CFD codes use the

finite-volume or finite-element methods which are better suited for modeling flow past complex geometries. For example, the FLUENT code uses the finite-volume method whereas ANSYS uses the finite-element method. In what follows, the CFD solution process will be illustrated using the finite-volume method, which is the most popular method used in practice.

1.1.2.3 Discretization using the finite-volume method

Looking closely at the airfoil grid shown earlier, shows that it consists of quadrilaterals. In the finite-volume method, such a quadrilateral is commonly referred to as a “cell”. In 2D, one could also have triangular cells. In 3D, cells are usually hexahedrals, tetrahedrals, or prisms. In the finite-volume approach, the integral form of the conservation equations are applied to the control volume defined by a cell to get the discrete equations for the cell. The integral form of the continuity equation for steady, incompressible flow is

$$\int_S \vec{V}.\hat{n}dS = 0 \tag{1.8}$$

The integration is over the surface S of the control volume and $\hat{n}$ is the outward normal at the surface. Physically, this equation means that the net volume flow into the control volume is zero.

Consider the rectangular cell shown in Figure 1.13.

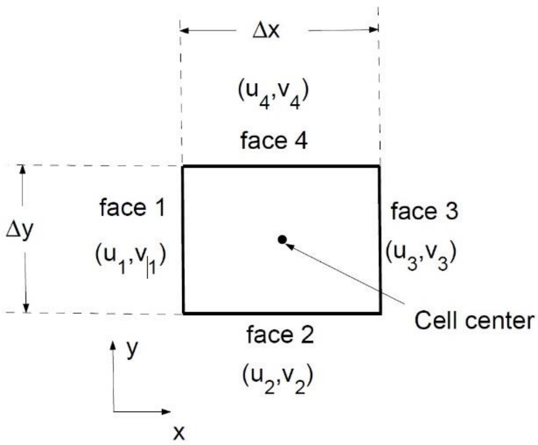

Figure 1.13 : A cell [9].

The velocity at face i is taken to be $V_i = u_i\hat{\imath} + v_i\hat{\jmath}$. Applying the mass conservation equation **(1.8)** to the control volume defined by the cell gives

$$-u_1\Delta y - v_2\Delta x + u_3\Delta y + v_4\Delta x = 0 \tag{1.9}$$

This is the discrete form of the continuity equation for the cell. It is equivalent to summing up the net mass flow into the control volume and setting it to zero. So it ensures that the net mass flow into the cell is zero i.e. that mass is conserved for the cell. Usually, though not always, the values at the cell centers are solved for directly by inverting the discrete system. The face values u_1, v_1, etc. are obtained by suitably interpolating the cell-center values at adjacent cells.

Similarly, one can obtain discrete equations for the conservation of momentum and energy for the cell. It will be described how to implement the finite-volume method for the momentum equations in the 1D example problem below. One can readily extend these ideas to any general cell shape in 2D or 3D and any conservation equation.

1.1.2.4 Example problem

Let us consider the classic problem of a viscous fluid flowing in a channel (Figure 1.9) under a constant applied pressure gradient $\frac{dp}{dx}$. We consider a fully developed, unidirectional flow so that the velocity u is only a function of the vertical coordinate y. Under these assumptions, the Navier-Stokes equations can be simplified to the following single governing equation (x-momentum)

$$0 = -{}^{dp}/_{dx} + \mu \frac{d^2u(y)}{dy^2} \qquad -1 \leq y \leq 1 \tag{1.10}$$

with boundary conditions given by the no-slip condition at the two channel walls as follows:

$$u(y) = 0 \; at \; y = \pm 1 \tag{1.11}$$

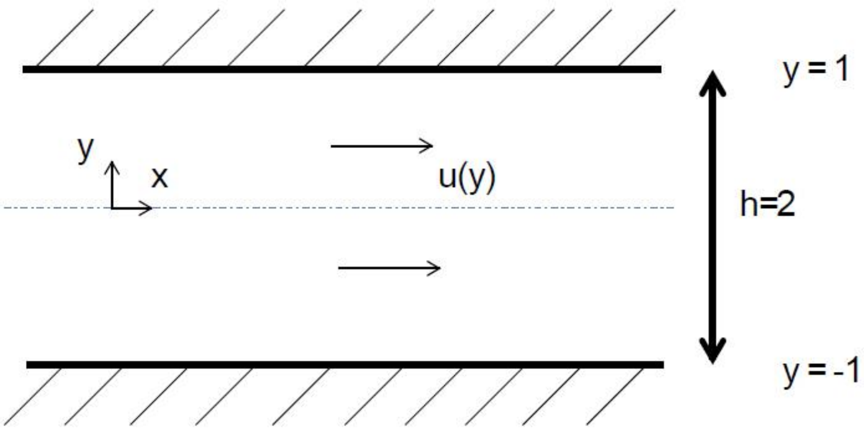

Figure 1.14 : A one direction flow between two walls [9].

Equations **(1.10)** and Equation **(1.11)** constitute a boundary value problem (BVP) which is to be solved numerically.

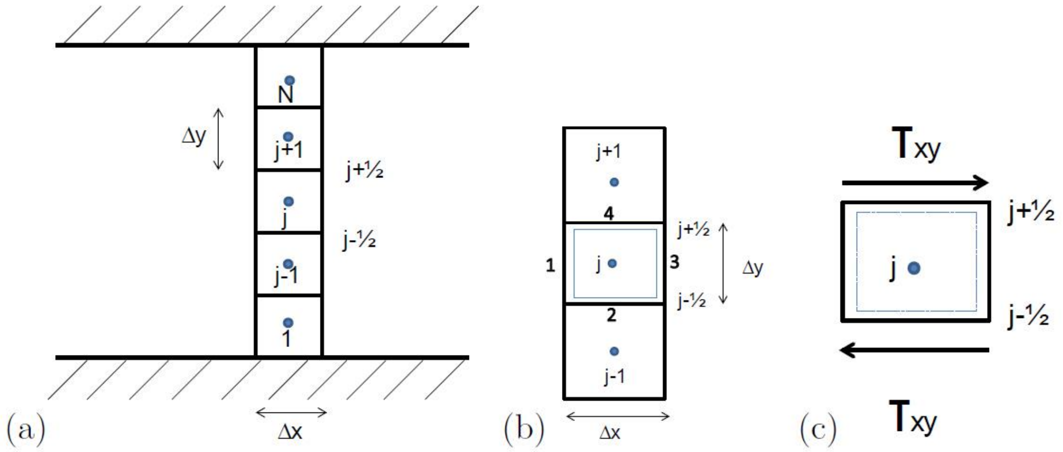

Figure 1.15 : Discretized flow in vertical direction [9].

1.1.2.5 Discretization using finite-volume method

In this section, we will describe the discretization of Equation **(1.10)** using the finite-volume (FV) scheme, similar to what FLUENT would do. Let's divide the vertical extent of the domain into N cells each having a height y and arbitrary width x as shown in Figure 1.15-a. The FV method involves writing out the integral form of the governing equations over a discrete control volume j (CV_j) and then using the divergence theorem to convert it into a surface integral around the control surface (CV_j), which we then evaluate using discrete values of the variable at the center of each cell (note that this is the cell-centered approach employed by FLUENT. A node-centered approach also exists but will not be discussed here). Referring to Figure 1.15-a, one can write Equation **(1.10)** as

$$0 = \int_{CV_j} \left(-{}^{dp}/_{dx}\right) dV_j + \int_{CV_j} \mu \frac{d^2u(y)}{dy^2} dV_j \qquad \textbf{(1.12)}$$

Since $\dfrac{dp}{dx}$ is a constant, the first-term on the RHS is really simple to deal with and will be discussed later. Let's concentrate on the second term

$$\int_{CV_j} \mu \frac{d^2u(y)}{dy^2} dV_j \qquad \textbf{(1.13)}$$

Using divergence theorem,

$$\int_{CV_j} \mu \frac{d^2u(y)}{dy^2} dV_j = \int_{CV_j} \nabla^2 u dV_j = \int_{CV_j} \nabla u.\hat{n} dS_j \qquad \textbf{(1.14)}$$

where $\hat{n}$ is the outward normal to the control surface. Let's traverse the the control surfaces of CV_j in CCW sense. Referring to Figure 1.15, we have

$$\int_{CV_j} \nabla u.\hat{n} dS_j = \int_{CV_1} \nabla u.\hat{n} dS_1 + \int_{CV_2} \nabla u.\hat{n} dS_2 + \int_{CV_3} \nabla u.\hat{n} dS_3 + \int_{CV_4} \nabla u.\hat{n} dS_4 \quad \textbf{(1.15)}$$

With respect to the axes provided in Figure 1.14, it's seen that the outward normal $\hat{n}$ to the surface is opposite to the direction of gradient for surfaces 1 and 2 and aligned with it for surfaces 3 and 4. Also, since the flow is fully developed, there are no net fluxes in the horizontal direction, i.e, through surface 1 and 3. Therefore, it can be written now for any interior cell j,

$$\int_{CV_j} \nabla u.\hat{n} dS_j = 0 + \int_{CV_2} \nabla u.\hat{n} dS_2 + \int_{CV_3} \nabla u.\hat{n} dS_3 + 0$$

$$= -(\frac{du}{dy})_{j-\frac{1}{2}} \Delta x + -(\frac{du}{dy})_{j+\frac{1}{2}} \Delta x$$

$$= -(\frac{u_j - u_{j-1}}{\Delta y}) \Delta x + \frac{u_{j+1} - u_j}{\Delta y} \Delta x$$

$$= \left(u_{j-1} - 2u_j + u_{j+1}\right) \frac{\Delta x}{\Delta y} \quad \textbf{(1.16)}$$

This term (multiplied by μ) is essentially a sum of the shear forces acting on the control volume CV_j as shown in Figure 1.15-c which is balanced by the pressure force. Notice that a central differencing scheme has been used to evaluate the fluxes at the interface of adjacent cells. Other schemes can be used as well but it is worth noting that this choice may influence spatial discretization error. More on that in a bit. But first let's complete discretization of Equation **(1.12)** by considering the first term on the LHS. Since $\frac{dp}{dx}$ is a constant, one can write,

$$\int_{CV_j} \left(-{}^{dp}/_{dx}\right) dV_j = \left(-{}^{dp}/_{dx}\right) V_j = \left(-{}^{dp}/_{dx}\right) \Delta x \Delta y \quad \textbf{(1.17)}$$

Therefore, putting everything together we get the discretized form of Equation **(1.12)** as

$$0 = \left(-{}^{dp}/_{dx}\right) \Delta x \Delta y + \mu(u_{j-1} - 2u_j + u_{j+1}) \frac{\Delta x}{\Delta y} \quad \textbf{(1.18)}$$

Dividing by $\Delta x \Delta y$, final discretized form is as

$$0 = \left(-{}^{dp}/_{dx}\right) + \frac{\mu(u_{j-1} - 2u_j + u_{j+1})}{(\Delta y^2)} \quad \textbf{(1.19)}$$

1.1.2.6 Assembly of discrete system and boundary conditions' application

In order to make calculations simple, let's assume $\frac{dp}{dx} = -1$ corresponding to a flow in the positive x direction and $\mu = 1$ and consider a discretization involving N = 3 cells as shown in Figure 1.16-a. Then, final discretized form for an interior cell becomes

$$u_{j-1} - 2u_j + u_{j+1} = -(\Delta y)^2 \tag{1.20}$$

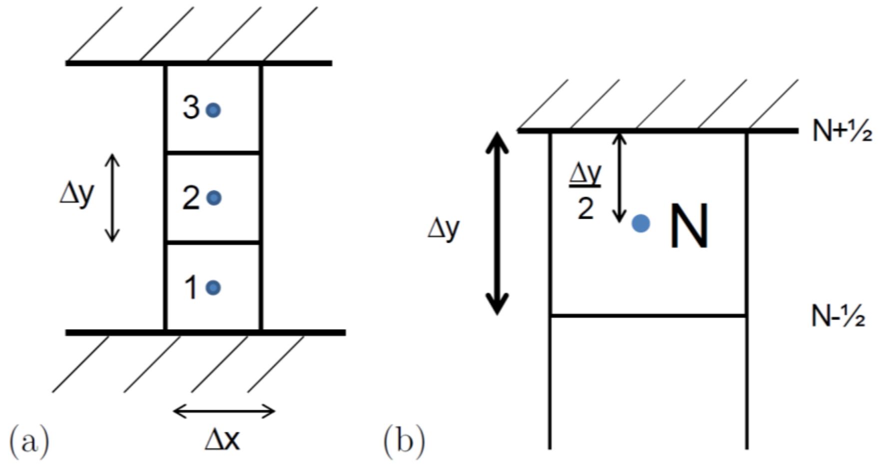

Figure 1.16 : Example problem: Discretization [9].

As discussed earlier, this equation is true as long as the cell (or control volume) is not adjacent to the boundary. For the boundary cells ($j = 1\ ve\ j = N$, Figure 1.16-a), it's needed to slightly modify the way fluxes calculation in order to accommodate the boundary points $N + \frac{1}{2}$ and $N - \frac{1}{2}$. Referring to Figure 1.16-b, it can be seen that for $j = N$,

$$\int_{CS_N} \nabla u.\hat{n} dS_N = -\frac{u_N - u_{N-1}}{\Delta y}\Delta x + \frac{u_{N+\frac{1}{2}} - u_n}{\Delta y/_2}\Delta x = (u_{N-1} - 3u_N + 2u_{N+\frac{1}{2}})\frac{\Delta x}{\Delta y} \tag{1.21}$$

Since for $J = N$, there are no points corresponding to $N + 1$, the boundary point $N + \frac{1}{2}$ has been used to compute the flux. The same tactic can be employed for the bottom boundary cell $j = 1$. Therefore, for $N = 3$ cells, our final discretized set of equations corresponding to the governing Equation **(1.10)** is

$$2u_{1-\frac{1}{2}} - 3u_1 + u_2 = -(\Delta y)^2 \qquad (j = 1) \tag{1.22}$$

$$u_1 - 2u_2 + u_3 = -(\Delta y)^2 \qquad (j = 2) \tag{1.23}$$

$$u_2 - 3u_3 + 2u_{3+\frac{1}{2}} = -(\Delta y)^2 \qquad (j = 3) \qquad \textbf{(1.24)}$$

These equations form a system of three simultaneous algebraic equations in the three unknowns (u_1, u_2, u_3) with specified boundary values $(u_{1-\frac{1}{2}}, u_{3+\frac{1}{2}})$, for which the no-slip boundary conditions $u_{1-\frac{1}{2}} = u_{3+\frac{1}{2}} = 0$ can be applied immediately . In this case, one can solve these equations by inspection, but for practical systems it is needed to use a large number of cells. Therefore, it is generally convenient to write this system in matrix form:

$$\begin{pmatrix} -3 & 1 & 0 \\ 1 & -2 & 1 \\ 0 & 1 & -3 \end{pmatrix} \begin{pmatrix} u_1 \\ u_2 \\ u_3 \end{pmatrix} = -(\Delta y)^2 \begin{pmatrix} 1 \\ 1 \\ 1 \end{pmatrix} \qquad \textbf{(1.25)}$$

Now, one can easily see how the system would look like as more and more cells are added. For example, if one has $N = 5$, he would have the following system:

$$\begin{pmatrix} -3 & 1 & 0 & 0 & 0 \\ 1 & -2 & 1 & 0 & 0 \\ 0 & 1 & -2 & 1 & 0 \\ 0 & 0 & 1 & -2 & 1 \\ 0 & 0 & 0 & 1 & -3 \end{pmatrix} \begin{pmatrix} u_1 \\ u_2 \\ u_3 \\ u_4 \\ u_5 \end{pmatrix} = -(\Delta y)^2 \begin{pmatrix} 1 \\ 1 \\ 1 \\ 1 \\ 1 \end{pmatrix} \qquad \textbf{(1.26)}$$

In a general situation therefore, one would apply the discrete equations to the cells in the interior of the domain. For the cells adjacent to the boundary (or in some cases, near the boundary), one would apply a combination of the discrete equations and boundary conditions. In the end, one would obtain a system of simultaneous algebraic equations with the number of equations being equal to the number of independent discrete variables.

1.1.2.7 Solution of discrete system

The discrete system of Equation **(1.25)** for 1D example can be easily inverted to obtain the unknowns at the grid points. $\Delta y = {}^{2}/_{3}$, it can be solved for $u_{1,} u_2 \; and \; u_3$ in turn and obtain

$$u_1 = {}^{1}/_{3} \quad u_2 = {}^{5}/_{9} \quad u_3 = {}^{1}/_{3} \qquad \textbf{(1.27)}$$

The exact or analytical solution for this problem is easily calculated to be

$$u_{exact}(y) = -{}^{y^2}/_{2} + {}^{1}/_{2} \qquad \textbf{(1.28)}$$

Figure 1.17 shows the comparison of the discrete solution obtained on the three-cell grid along with the exact solution. Verify that the relative error is largest at the cells 1 and 3 each being equal to 20%.

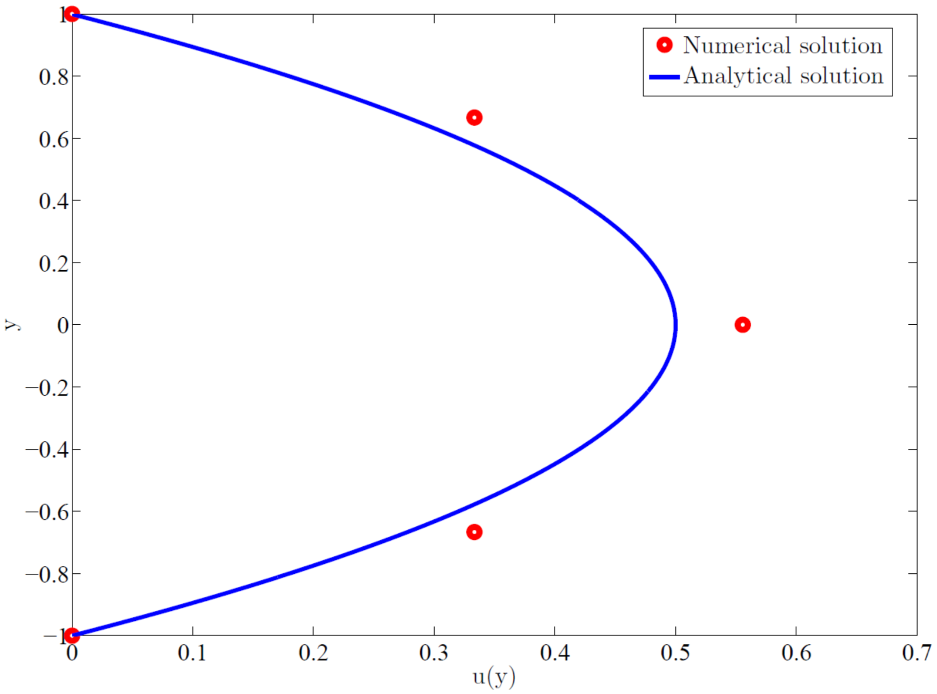

Figure 1.17 : Numerical and analytical results comparison [9].

In a practical CFD application, one would have thousands to millions of unknowns in the discrete system and if one uses, say, a Gaussian elimination procedure naively to invert the matrix. So a lot of work goes into optimizing the matrix inversion in order to minimize the CPU time and memory required. The matrix to be inverted is usually sparse i.e., most of the entries in it are zeros since the discrete equation at a grid point or cell will contain only quantities at the neighboring points or cells; verify that this will indeed be the case for matrix system as we increase the number of cells N . A CFD code would store only the non-zero values to minimize memory usage. It would also generally use an iterative procedure to invert the matrix; the longer one iterates, the closer one gets to the true solution for the matrix inversion.

1.1.2.8 Grid convergence

It will be shown later that the spatial discretization error in our finite-volume approximation of **(1.10)** is $O(\Delta y^2)$. This means that as the number of cells is increased, Δy will be decreased which should lead to reduction in the numerical discretization error.

Let's consider the effect of increasing the number of cells N on the numerical solution. $N = 5, N = 10\ and\ N = 20$ will be considered in addition to the $N = 3$ case solved previously. The above assembly and solution steps will be repeated on each of these additional grids. The resulting discrete system was solved using MATLAB. The following figure compares the results obtained on the four grids with the exact solution. As can be see by inspection, the numerical solution becomes better and better as the number of cells is increased.

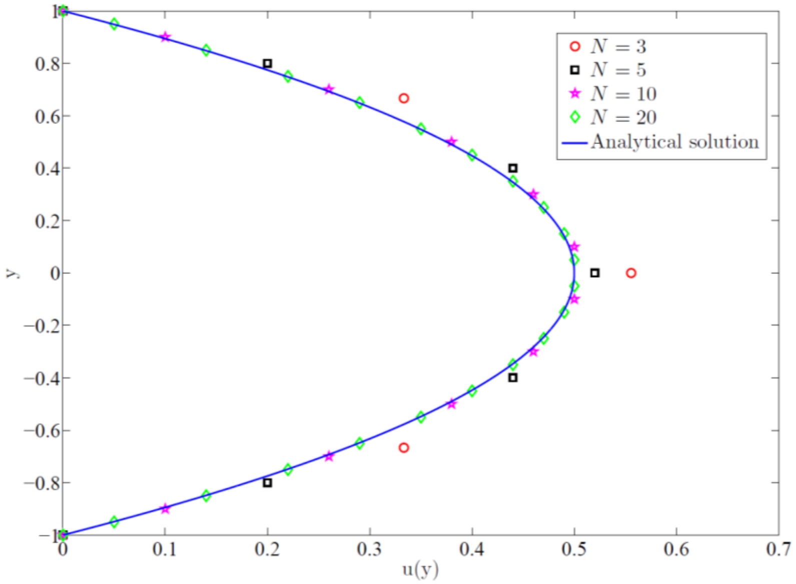

Figure 1.18 : Results comparison for calculations of 3, 5, 10 and 20 cells [9].

When the numerical solutions obtained on different grids agree to within a level of tolerance specified by the user, they are referred to as 'grid converged' solutions. It is very important to investigate the effect of grid resolution on the solution in every CFD problem which is solved.

1.1.2.9 Discretization error

It is mentioned earlier that the discretization error for the scheme is $O(\Delta y^2)$. It can be seen that this is so using a Taylor series expansion. Recall that the flux at interface $j + \frac{1}{2}$ of cell j was given by

$$\left(\frac{du}{dx}\right)_{j+\frac{1}{2}} = \frac{u_{j+1} - u_j}{\Delta y} \quad \textbf{(1.29)}$$

Let's now consider the Taylor series expansions of u_{j+1} and u_j about some value $u_{j+\frac{1}{2}}$.

$$u_{j+1} = u_{j+\frac{1}{2}} + (\Delta y/2)\left(\frac{du}{dx}\right)_{j+\frac{1}{2}} + \frac{(\Delta y/2)^2}{2}\left(\frac{d^2u}{dx^2}\right)_{j+\frac{1}{2}} + O(\Delta y^3)$$

$$u_j = u_{j+\frac{1}{2}} + (-\Delta y/2)\left(\frac{du}{dx}\right)_{j+\frac{1}{2}} + \frac{(-\Delta y/2)^2}{2}\left(\frac{d^2u}{dx^2}\right)_{j+\frac{1}{2}} + O(\Delta y^3) \qquad \textbf{(1.30)}$$

Here, $O(\Delta y^3)$ indicates that in the series of terms that follow, the term containing the cubic power of Δywill dominate. This is because Δy<<1, which is a necessary condition to write a Taylor series expansion. Subtracting the two, terms with even powers of Δy cancel and odd powers of Δy add up to give,

$$u_{j+1} - u_j = 2(\Delta y/2)\left(\frac{du}{dx}\right)_{j+\frac{1}{2}} + O(\Delta y^3)$$

$$\Rightarrow \left(\frac{du}{dx}\right)_{j+\frac{1}{2}} = \frac{u_{j+1}-u_j}{\Delta y} + O(\Delta y^2) \qquad \textbf{(1.31)}$$

Hence, it is seen that teh discretization scheme is second-order accurate in space i.e., it has an error that is of $O(\Delta y^2)$. Notice that the error in a finite-difference approximation (in this case, a central difference scheme) used as part of the finite volume discretization.

1.1.2.10 Dealing with nonlinearity

Just for a moment, consider the above flow but now in the developing region of the channel i.e., the flow is not yet fully developed but still steady under a constant pressure gradient. All channel flows will contain a section near the entrance where the flow is not fully developed. Boundary layers start growing on the upper and lower channel walls and the flow can become fully developed only after those two layers have merged. The Navier-Stokes equations along the x-direction for the velocity field (now 2D, $\vec{V} = [u, v]$) for such a developing flow can be written as

$$u\frac{\partial u}{\partial x} + v\frac{\partial u}{\partial z} = -\left({}^{1}/_{\rho}\right){}^{dp}/_{dx} + v\left(\frac{\partial^2 u}{\partial x^2} + \frac{\partial^2 u}{\partial y^2}\right) \qquad \textbf{(1.32)}$$

Such an equation is non-linear due to the convection terms $\frac{\partial u}{\partial x}$ and $v\frac{\partial u}{\partial y}$, where a product of two functions of the dependent variable is given. Therefore, one has to almost always deal with non-linearity when dealing with the momentum conservation equation for a fluid due to the convection term, which in vector form looks like $\overrightarrow{(V.\nabla)}\vec{V}$. Phenomena such as turbulence and chemical reaction introduce additional nonlinearities. The highly nonlinear nature of the governing equations for a fluid makes it challenging to obtain accurate numerical solutions for complex flows of practical interest.

In example above, the effect of non-linearity and how to handle it can be demonstrated by con- side ring an additional body force per unit volume $-\alpha u^2$ acting on the fluid, where α is a constant. Such forces are not common for normal fluids, but can be observed for exotic fluids like Ferro fluids which respond to magnetic fields. Our governing equation, therefore, is modified to

$$0 = -dp/dx + \mu \frac{d^2u(y)}{dy^2} - \alpha u(y)^2 \quad -1 \leq y \leq 1 \qquad \textbf{(1.33)}$$

The finite-volume approximation can be determined to this equation following the method described previously. The additional non-linear term can be discretized assuming a constant value of u in each cell i.e.,

$$\int_{CV_j} -\alpha u^2 dV_j = -\alpha u^2 V_j = -\alpha u^2 \Delta x \Delta y \qquad \textbf{(1.34)}$$

Therefore, the discretized equation for each interior cell is given by

$$0 = (dp/dx) + \mu \frac{u_{j-1} - 2u_j + u_{j+1}}{(\Delta y)^2} - \alpha u_j^2 \qquad \textbf{(1.35)}$$

This is a nonlinear algebraic equation with the u_j^2 term being the source of the nonlinearity.

The strategy that is adopted to deal with nonlinearity is to linearize the equations about a guess value of the solution and to iterate until the guess agrees with the solution to a specified tolerance level. We will illustrate this on the above example. Let u_{gj} be the guess for u_j. Define

$$\Delta u_j = u_j - u_{gj} \qquad \textbf{(1.36)}$$

Rearranging and squaring this equation gives

$$u_j{}^2 = u_{gj}^2 + 2u_{gj}\Delta u_j + \left(\Delta u_j\right)^2 \qquad \textbf{(1.37)}$$

Assuming that $\Delta u_j \ll u_{gj}$ (it is desired to iterate until this condition is satisfied), the Δu_j^2 term can be neglected to get

$$u_j{}^2 \simeq u_{gj}^2 + 2u_{gj}\Delta u_j = u_j{}^2 = u_{gj}^2 + 2u_{gj}\left(u_j - u_{gj}\right) \qquad \textbf{(1.38)}$$

Thus,

$$u_j{}^2 \simeq 2u_{gj}u_j - u_{gj}^2 \qquad \textbf{(1.39)}$$

After linearization, the discretized equations become

$$0 = (dp/dx) + \mu \frac{u_{j-1} - 2u_j + u_{j+1}}{(\Delta y)^2} - \alpha\left(2u_{gj}u_j - u_{gj}^2\right) \qquad \textbf{(1.40)}$$

Since the error due to linearization is $O(\Delta y^2)$ (remember that is the term which had been neglected), it will tend to zero as $u_g \rightarrow$ u.

In order to calculate the finite-volume approximation (Equation **(1.40)**), guess values of u_g are needed at the grid points. It will be started with an initial guess value in the first iteration. For each subsequent iteration, the u value obtained in the previous iteration is used as the guess value. Iteration 1: $u_g^{(1)}$= Initial guess

Iteration 2: $u_g^{(2)}= u^{(1)}$

⋮

Iteration m: $u_g^{(m)} = u^{(m-1)}$

The superscript indicates the iteration level. The iterations will be continued until they converge. The discussion will be differed on how to evaluate convergence until a little later.

This is essentially the process used in CFD codes to linearize the nonlinear terms in the conservations equations, with the details varying depending on the code. The important points to remember are that the linearization is performed about a guess and that it is necessary to iterate through successive approximations until the iterations converge.

1.1.2.11 Direct and Iterative solvers

It was seen that it is needed to perform iterations to deal with the nonlinear terms in the governing equations. Another factor will be discussed that makes it necessary to carry out iterations in practical CFD problems.

Verify that the discrete equation system resulting from the finite-volume approximation (Equation **(1.40)**) on the three-cell grid is

$$\begin{pmatrix} -3 - 2\alpha u_{gj}\Delta y^2 & 1 & 0 \\ 1 & -2 - 2\alpha u_{gj}\Delta y^2 & 1 \\ 0 & 1 & -3 - 2\alpha u_{gj}\Delta y^2 \end{pmatrix} = -(\Delta y^2)\begin{pmatrix} 1 - \alpha u_{gj}^2 \\ 1 + \alpha u_{gj}^2 \\ 1 + \alpha u_{gj}^2 \end{pmatrix}$$

$$Au = b \qquad \textbf{(1.41)}$$

Note that one can write the discretized system of equations as the standard linear system with the coefficient matrix A, vector of unknowns u and the RHS vector b. In a practical problem, one would usually have thousands to millions of grid points or cells so that each dimension of the above matrix would be of the order of a million (with most of the elements being zeros). Inverting such a matrix directly would take a prohibitively large amount of memory. So instead, the matrix is inverted using an iterative scheme as discussed below.

The finite-volume approximation (Equation **(1.42)**) can be rearranged on an interior cell j so that u_j is expressed in terms of the values at the neighboring cells and the guess values:

$$u_j = \frac{\Delta y^2\left(1+\alpha u_{gj}^2\right)+u_{j-1}+u_{j+1}}{2+2\alpha u_{gj}\Delta y^2} \quad \textbf{(1.42)}$$

A similar equation can be written for the boundary cells as well. Here, the Gauss-Siedel iterative technique is considred for solving the linear system of equations (Equation **(1.41)**) one at a time starting from a guessed solution and using results from the most recent iteration as soon as they become available. For example, if a neighboring value at the current iteration level is not available, the value at the previous iteration is used but if it has already been computed for the present iteration, the current value is used. Let's say that one sweep from the bottom to the top of the grid i.e., one updates u_1 first, based on the value of u_1 and u_2 at the previous iteration. In the next step, when one updates u_2, the previous iteration for u_3 and u_2 is used; but for u_1 the value already computed in the current iteration would be used, and so on. Thus, in the m^{th} iteration, u_{j+1}^m and u_j^m is not available while u_j^{m-1} is. Therefore, one uses the previous iteration values as the guess values $u_{gj}^m = u_j^{m-1}$ and u_{j+1}^{m-1} to get for the interior cells

$$u_j^m = \frac{\Delta y^2\left(1+\alpha\left(u_j^{m-1}\right)^2\right)+u_{j-1}^m+u_{j+1}^{m-1}}{2+2\alpha u_j^{m-1}\Delta y^2} \quad \textbf{(1.43)}$$

It is easy to see that for a boundary cell (for example j = 1), the update looks like

$$u_j^m = \frac{\Delta y^2\left(1+\alpha\left(u_j^{m-1}\right)^2\right)+u_{j+1}^{m-1}}{3+2\alpha u_j^{m-1}\Delta y^2} \quad \textbf{(1.44)}$$

Note that $u_{gy}^{m} = u_{j}^{m-1}$ is used to iterate for the non-linear terms whereas u_{j+1}^{m-1} and u_{j-1}^{m} are used to iterate for the matrix inversion. Since some chosen guess values are being used to start iteration (and previous iteration values as guesses thereafter) at neighboring points, only an approximate solution is being obtained for the inversion of the coefficient matrix A in Equation **(1.41)** during each iteration. But in the process, the memory required for the inversion has been greatly reduced. This tradeoff is good strategy since it does not make sense to expend a great deal of resources to do an exact matrix inversion when the matrix elements depend on guess values which are continuously being refined. Notice that 'in an act of cleverness', the iteration has been combined to handle nonlinear terms with the iteration for matrix inversion into a single iteration process. Most importantly, as the iterations converge and $u_g \rightarrow u$, the approximate solution for the matrix inversion tends towards the exact solution for the inversion since the error introduce by using u_g instead of u in Equation **(1.43)** tends to zero.

Once again, remember that in this case the iteration serves two purposes:

1. It allows for efficient matrix inversion with greatly reduced memory requirements.

2. It is necessary to solve nonlinear equations.

In steady problems, a common and effective strategy used in CFD codes is to solve the unsteady form of the governing equations and 'march' the solution in time until the solution converges to a steady value. In this case, each time step is effectively an iteration, with the guess value at any time step being given by the solution at the previous time step.

1.1.2.12 Iterative convergence

Recall that as $u_g \rightarrow u$, the linearization and matrix inversion errors trends to zero. So it is continued to iteration process until some selected measure of the difference between u_g and u, referred to as the residual, is 'small enough'. One could, for instance, define the residual R as the absolute value of the difference between u at time-step (or iteration number) 'm' with that at the previous time-step '$m-1$' summed over all the cells:

$$R \equiv \sum_{j-1}^{N} \left| u_j^m - u_j^{m-1} \right| \qquad \textbf{(1.45)}$$

It is useful to scale this residual in some way because an unscaled residual of, say, 0.01 would be relatively small if the average value of u in the domain is 5000 but would be relatively large if the average value is 0.1. Scaling ensures that the residual is a relative rather than an absolute measure. Scaling the above residual by dividing by the absolute sum of u over all the cells gives

$$R^u \equiv \frac{\sum_{j=1}^{N}\left|u_j^m - u_j^{m-1}\right|}{\sum_{j=1}^{N}\left|u_j^{m-1}\right|} \qquad \textbf{(1.46)}$$

In fact, this is the form of the residual that FLUENT uses for its pressure-based solver for momentum and scalar-transport equation. For full details on how FLUENT computes residuals in other cases, please refer to the user manual.

For the nonlinear example problem, the initial guess will be taken at each cell to be equal to zero (arbitrarily) i.e., $u_{gj}^{(1)} = 0$ for all j and consider $N = 10$ cells. In each iteration from here on, u is updated, going from cell $j = 1$ to $j = N$ using Equation **(1.43)** for the interior cells and Equation **(1.44)** for the boundary cells. The residual can be calculated using Equation **(1.46)** at each time-step and monitor it to determine convergence. Usually the iterations are terminated when the residual falls below some threshold value (for example, 10^{-6})), which is referred to as the convergence criterion. The variation of the residual with iterations obtained from MATLAB is shown below. Note that a logarithmic scale is used for the ordinate. Verify that the iterative process converges to residual level smaller than 10^{-6} in about 105 iterations. In more complex problems and/or with a more stringent convergence criterion, a lot more iterations would be necessary for achieving convergence.

The solution after 30, 60 and 90 iterations and the converged solution (105 iterations) are shown below along with the linear solution obtained previously. The solutions for iterations 90 and 105 are indistinguishable on the graph. This is another indication that the solution has converged. It can be seen that the negative force (in the x-momentum equation) on the system leads to a drag that reduces the velocities across the channel.Unfortunately, there isn't an analytical solution for this problem. Therefore, one should be careful not to trust the numerical solution blindly. The topic of verification and validation of the numerical solution is critically important to a CFD engineer. Also, one can easily evaluate whether the solution is grid converged or not by varying the number of cells N. Checking for solution convergence and grid convergence are the two most simple checks one can do to determine whether the numerical solution is correct or not.

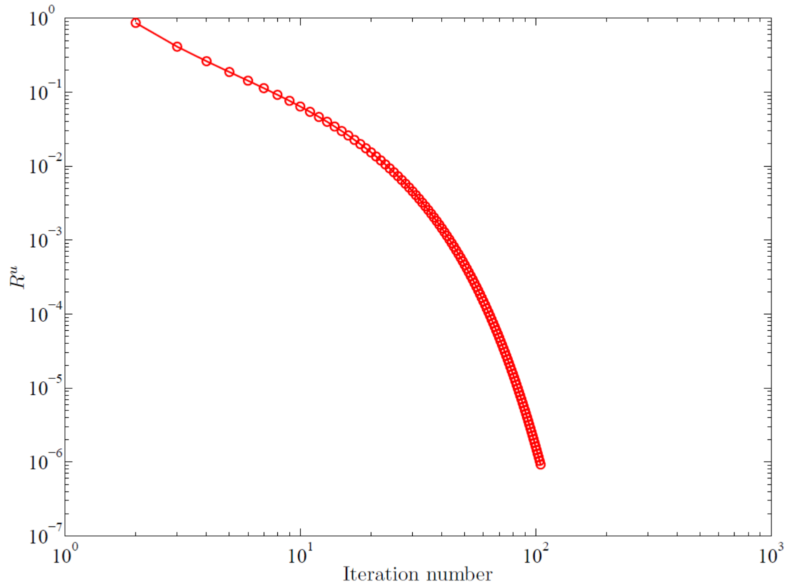

Figure 1.19 : Residual changes by iterations [9].

Another consideration is the comparison of the iterative convergence error, which is of order 10^{-6}, and the truncation error which is of order $\Delta y^2 \sim 10^{-2}$. So, although the residual is derived down to 10^{-6}, the accuracy of the solution is limited by the truncation error (of order 10^{-2}), which is a waste of computing resources. In a good calculation, both errors would be of comparable level and less than a tolerance level chosen by the user. Therefore, the numerical solution would get better on refining the grid so that truncation error does not dominate.

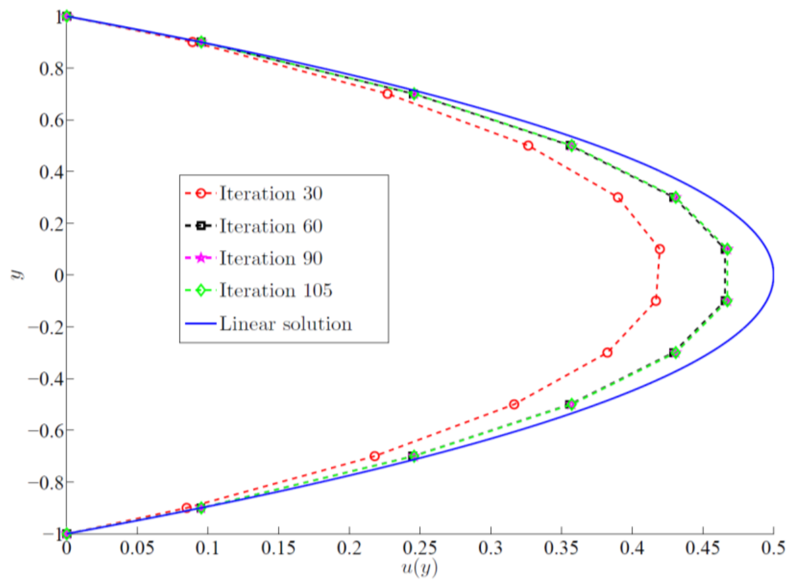

Figure 1.20 : Comparison of linear and iterative results [9].

2. DRAWER DESIGN PHASE

Drawer is one of the most important parts in spun-bond production system. Polymer which is now heated and slenderized, is guided to drawer to get cooler and thinner (Figure 2.1).

Figure 2.1 : Hot and slenderized polymer coming out of die.

The fluid used in this process is air. Firstly, air is sent into the drawer by a compressor (Figure 2.2); then it is guided into narrowing partitions to increase its speed; finally, it is sent to a narrower section which roles as a jet to bring into the place in which fiber drawing process is done (Figure 2.3).

In this section, air is brought into a drawer from two sided narrow jets which causes a negative pressure there. As a result, air velocity increases. Higher speed slenderizes fibers and guides them to the bottom of drawer. Fibers are cooled by coming down and become ready for next stage of the process.

Because of drawer sensitivity, its design has been made in different stages; beside of making new changes, cons and pros of every design have been investigated for every design.

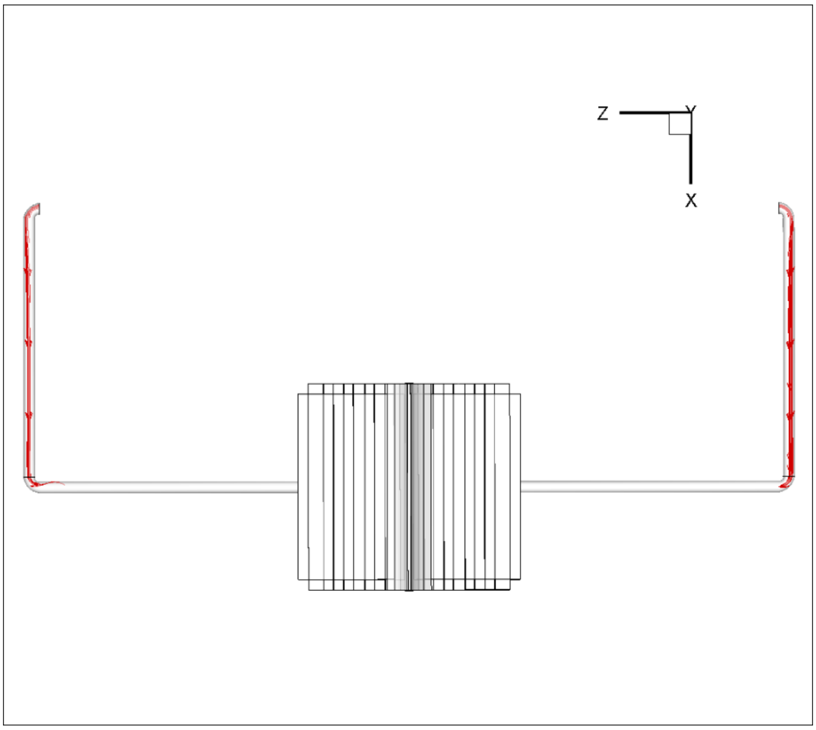

Figure 2.2 : Air is sent into fiber drawer by a compressor.

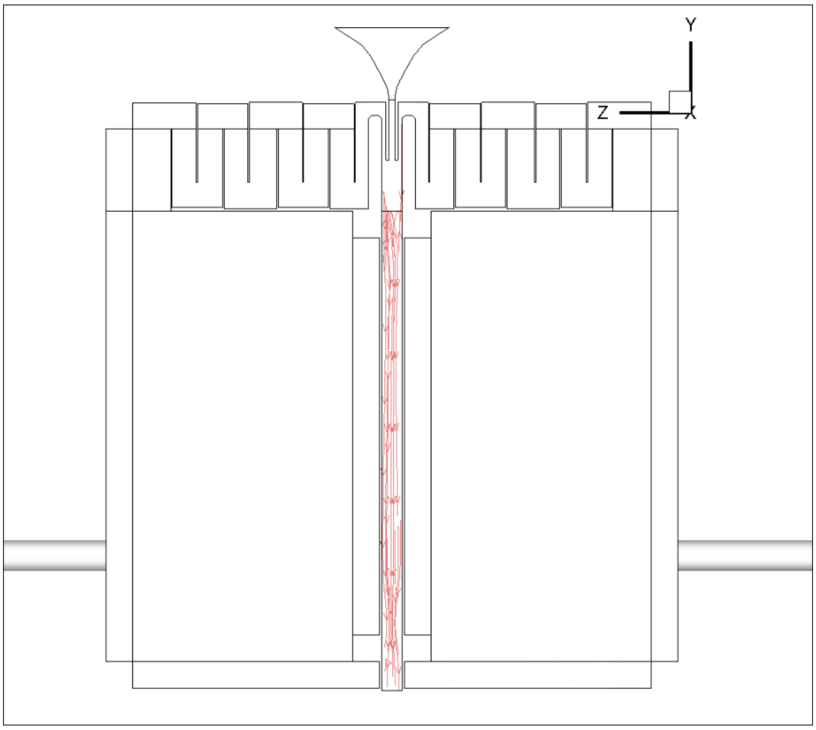

Figure 2.3 : Air exits from drawer after going through some stages.

2.1 Design Development Process

Figure 2.4 and Figure 2.5 show a pre-design of drawer which is created in a CAD software. High speed air could be provided by a centrifugal (radial) fan which is capable to provide high pressures. It is needed optimize parameters and also set conditions for different fibers and fabrics; so conveyor and die should have the capability of vertical moving; by this, it will be possible to adjust distances between die and drawer as well as conveyor and drawer. Air corridor should have the ability of widening and narrowing too. (Figure 2.6)

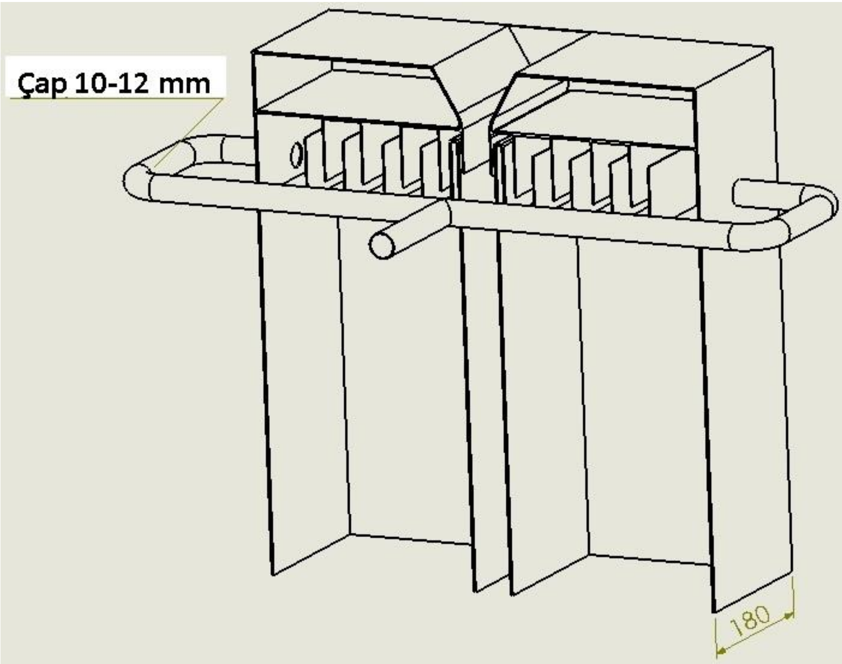

Figure 2.4 : Pre-design if pneumatic fiber drawing system.

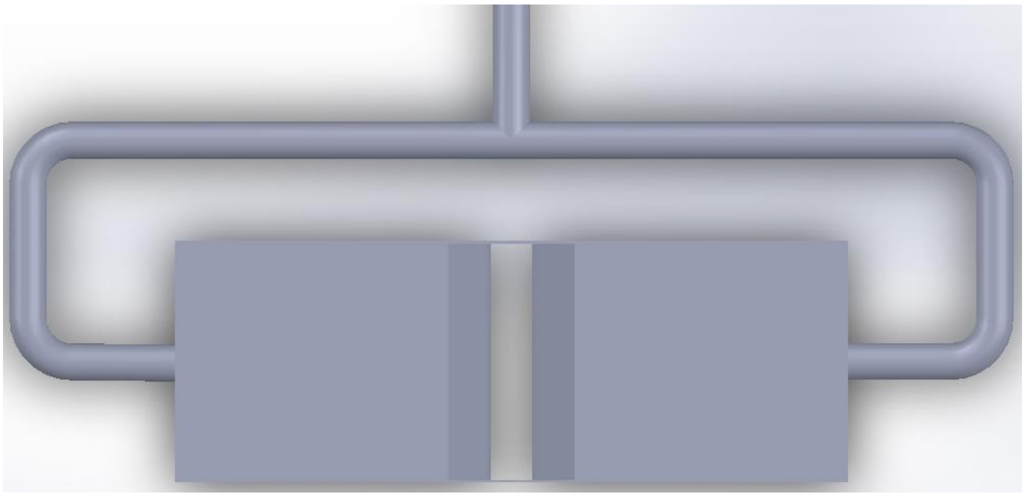

Figure 2.5 : Top view of pneumatic fiber drawing system.

Uniform air dispensation at jet section is an important factor as it will cause to a uniform drawing of fibers and consequently a uniform fabric. So a CFD analysis has been done on pre-design of attenuator and results is shown in Figure 2.7. A uniform air dispensation is obvious in mentioned figure.

Another CFD analysis has been done on air corridor which will contain fibers (Figure 2.8). As shown in Figure 2.8-a, a vacuum is formed at the exit section of jet. As a result, air is drawn into attenuator from top of system which is added to the air coming out of jet (Figure 2.8-b). By this, more air flow will be added to the system which will result in higher fiber drawing speeds.

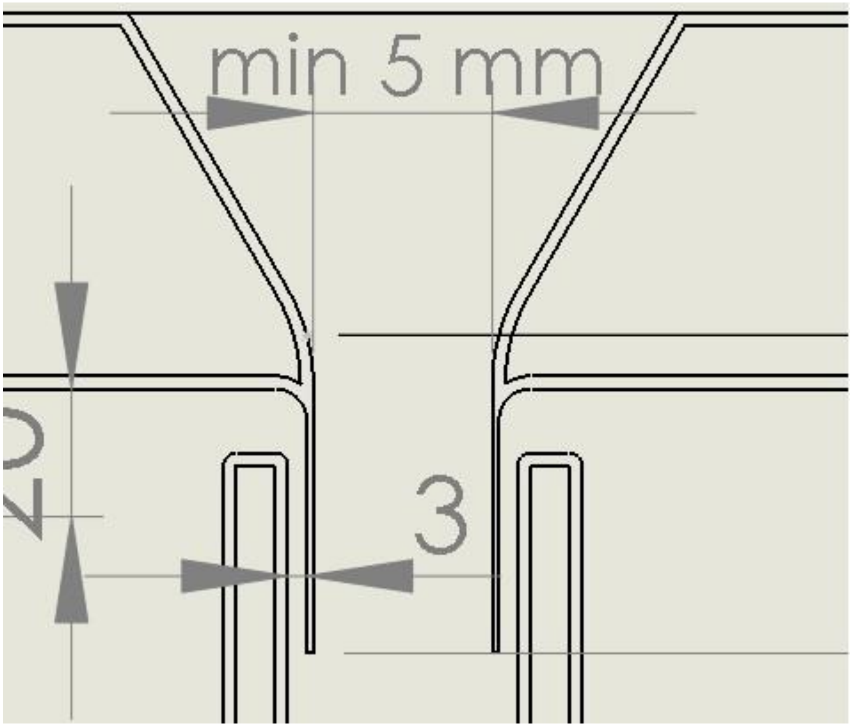

Figure 2.6 : Air jet at pre-design of pneumatic drawer system.

One of important factors in drawer design is its weight. With regard to this, aluminum has been chosen as the material and all of design process have been done as a function of this selection. It is mandatory to consider some limitation of aluminum during design process; for example it is possible to encontour with different problems if welding is applied to this material; so welding process should be diminished to the least possible.

As aluminum has low resistance, air speed or its pressure can deform material during drawing process; so it’s mandatory to use different supports in our design. Although using supports is very important, it shouldn’t eliminate aluminum usage cause, which was lightness of drawer unit. By considering these features and also different restrictions, a variety of design have been suggested.

The attenuator is formed by two air cases, which have same properties. Air and fiber passing section is formed by mounting two air cases next to each other (Figure 2.9)

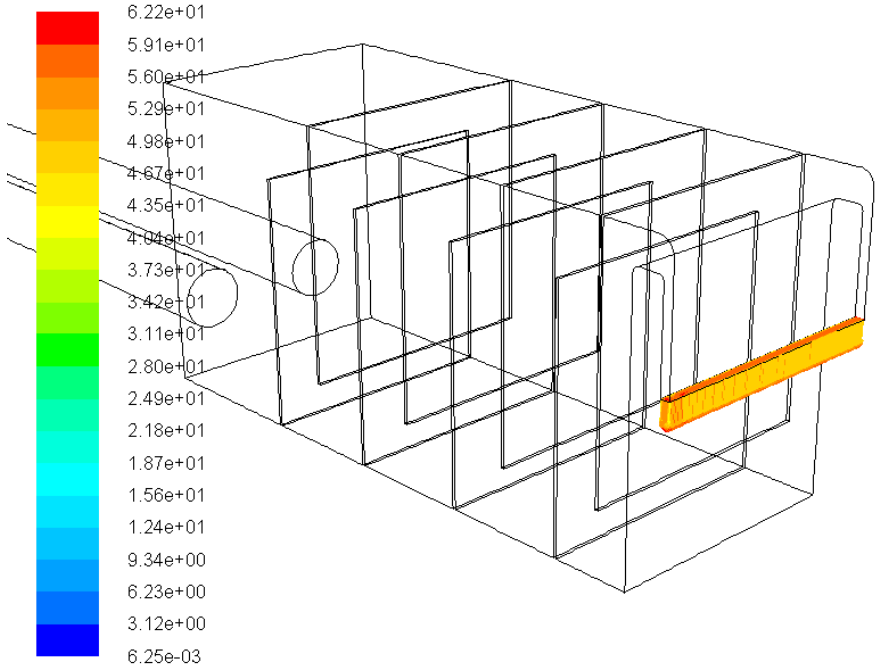

Figure 2.7 : Air contour at jet section obtained from CFD analysis (m/s).

As fluid geometry is symmetric, only on side is considered during analysis.

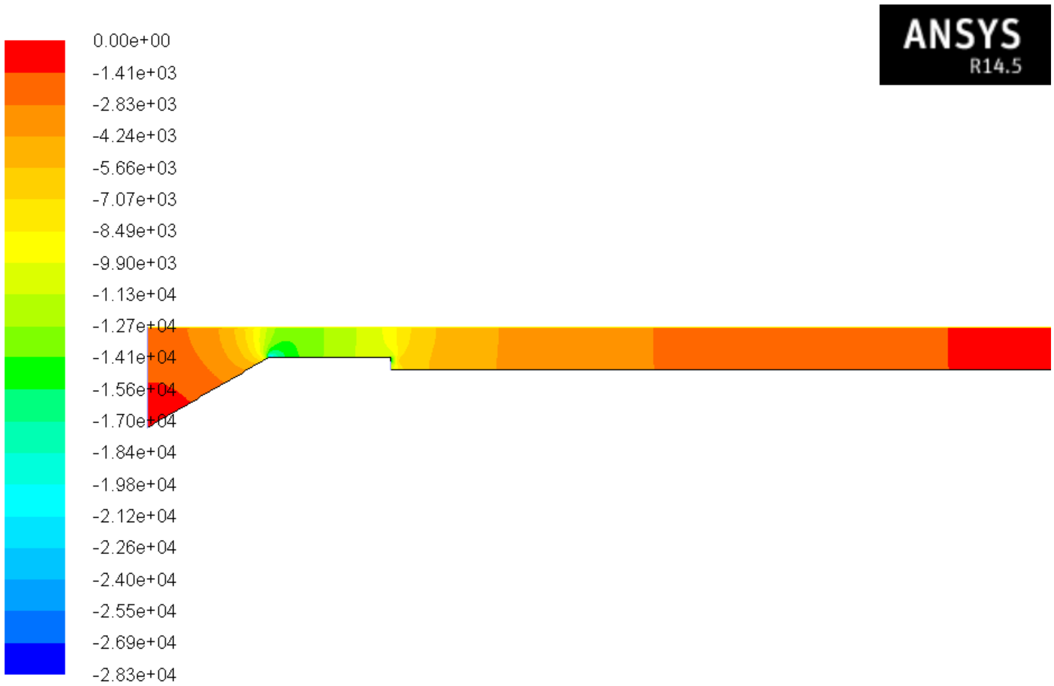

(a)

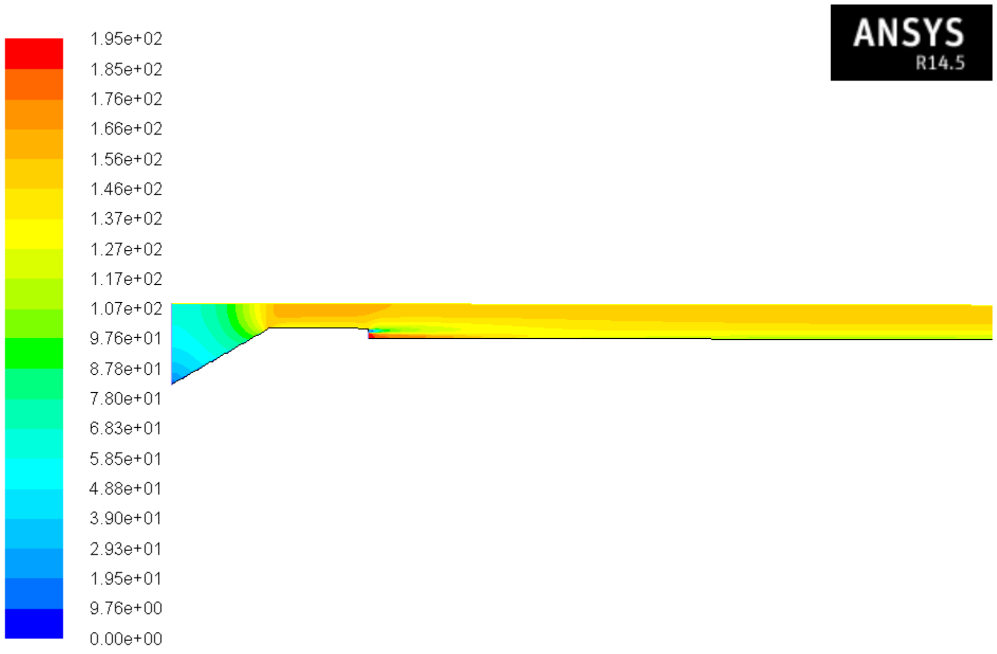

(b)

Figure 2.8 : a) pressure and b) velocity contours in pneumatic fiber drawing system.

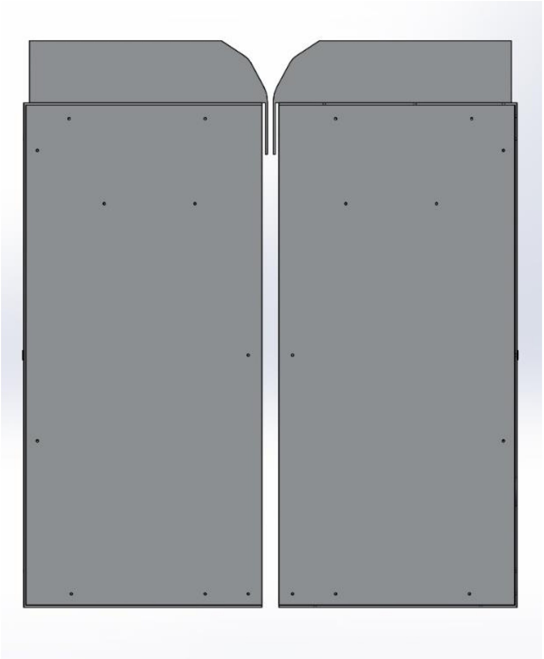

Figure 2.9 : Two air cases.

Firstly, it is suggested to use narrow bars of aluminum as an asset of resistance and vibration control. As shown in Figure 2.10, they are mounted on attenuators from outside of cases.

To consider air inlet, bars are separated into two parts at air entrance section.

Brackets are used as connection tools at 90 degree turns (Figure 2.11) and corners (Figure 2.12).

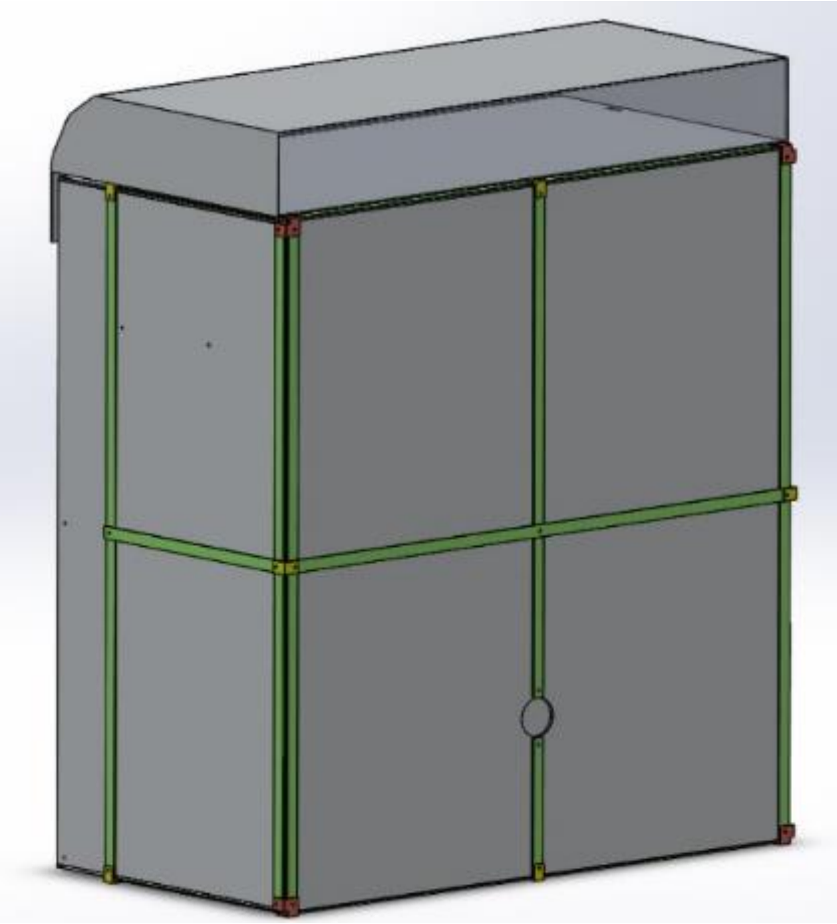

Figure 2.10 : Plates are supported by aluminum bars.

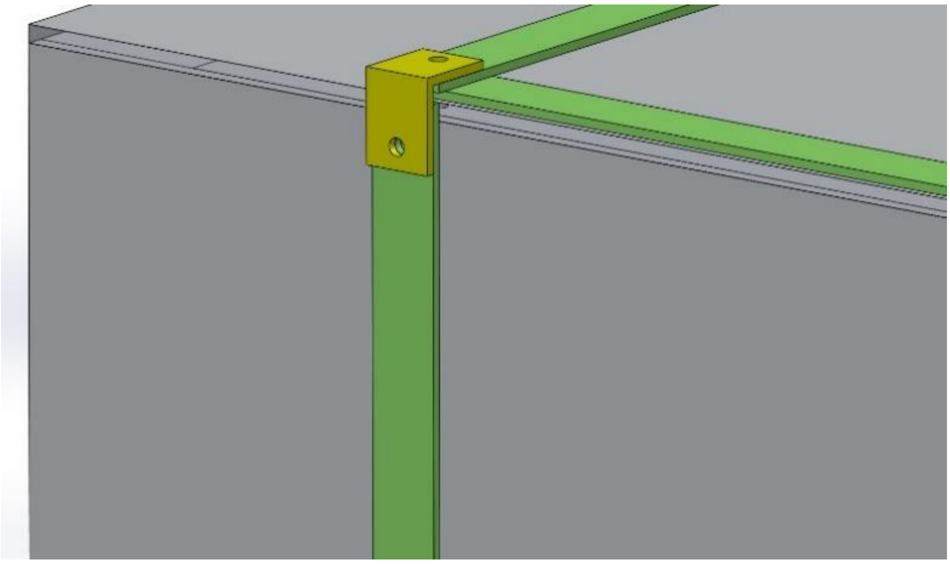

Figure 2.11 : 2D brackets.

To increase air velocity in cases, air channels with narrow cross sections have been designed. These air channels have been designed using four U profiles (Figure 2.13). Brackets are used as fastening tools between profiles and aluminum bars (Figure 2.14).

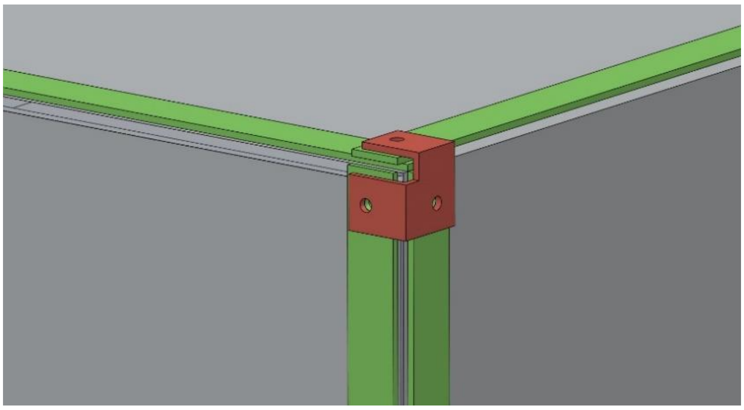

Figure 2.12 : 3D brackets.

Front panel is the most important part at case design stage. It should completely be flawless and smooth as it touches fibers. A tiny swelling or screw head can attach to fibers and prevent their movement. With regard to this, it should be welded to aluminum bars and also screwed to side aluminum profiles as well (Figure 2.14).

To strengthen air velocity between two cases, air should be brought smoothly into the passage; with regard to this, an air guide has been mounted on top of cases (Figure 2.15).

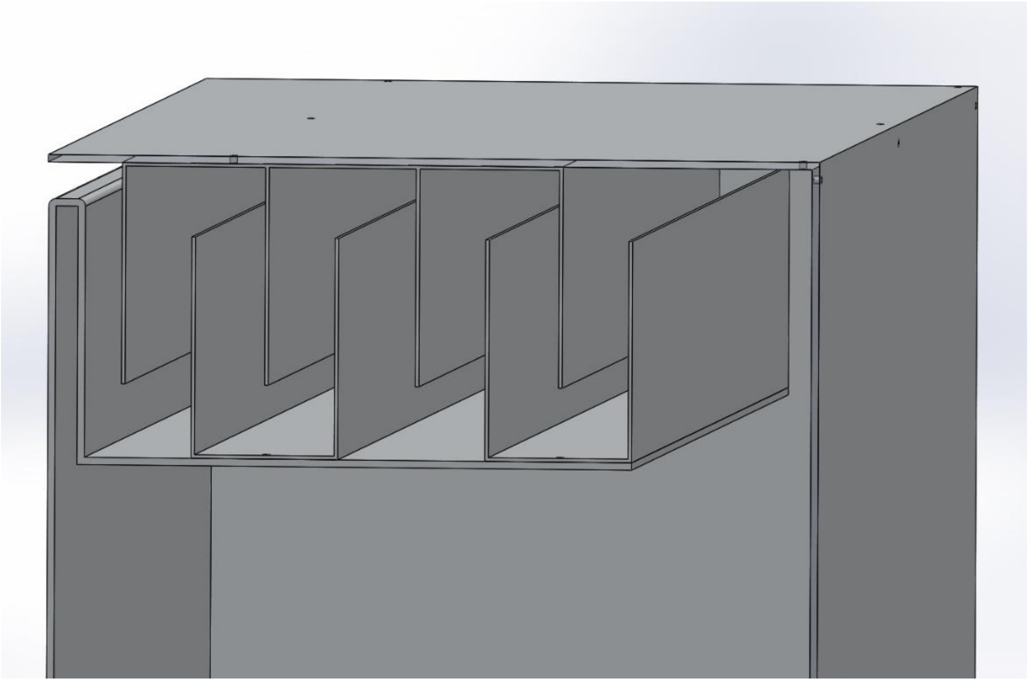

Figure 2.13 : U profiles used in air channels.

Jet part is also carried by air guide (Figure 2.16). The distance of this part should be adjustable in order to change air velocity; so air guide should have the capability of movıng forward and backward through the top side of cases. This feature can be obtained by widening screw holes which are opened at the bottom surface of air guide (Figure 2.17). As a result, jet distance could be adjusted by screw loosening and air guide movement.

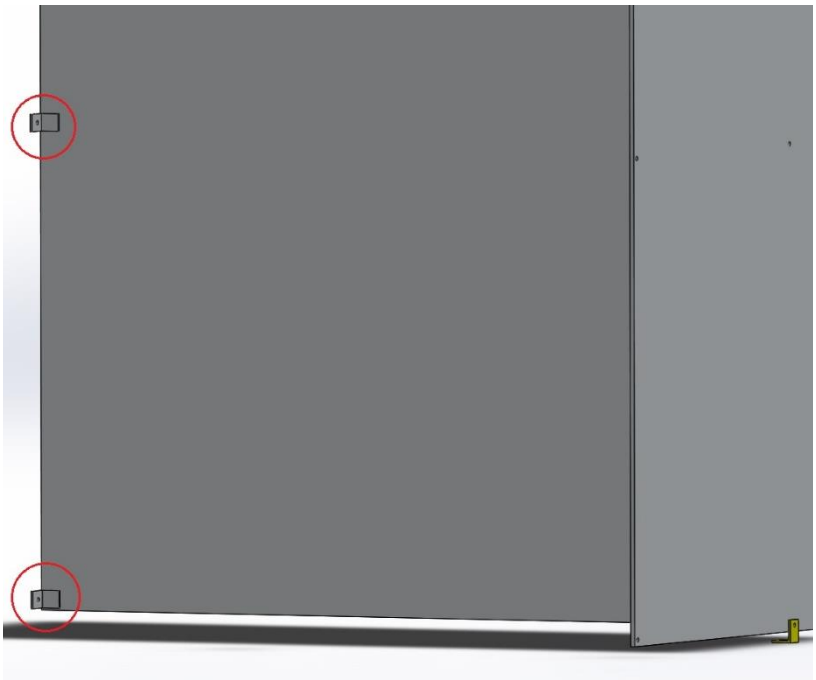

Figure 2.14 : Brackets are welded to front plates.

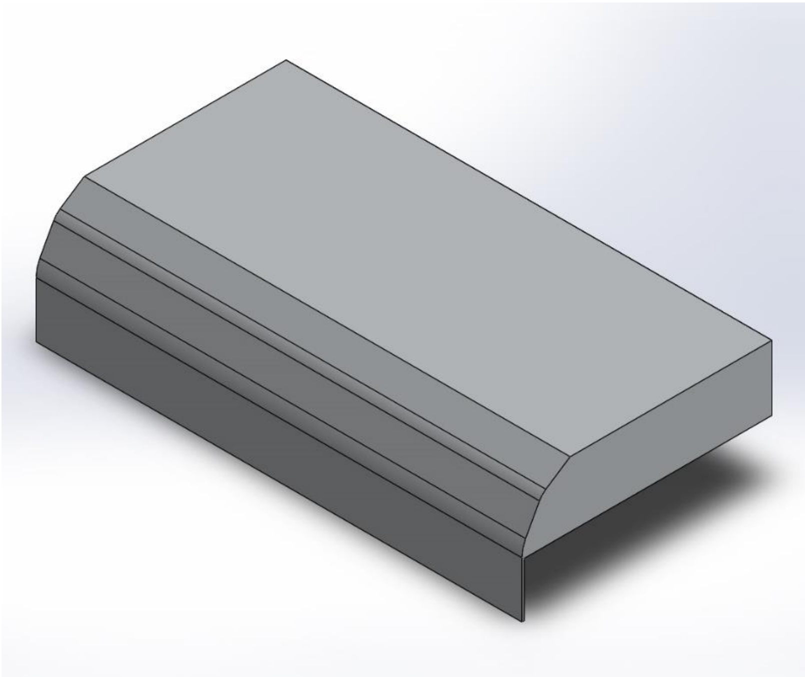

Figure 2.15 : Air guide.

This design is considered as first offer; at next stage it's evaluated in manufacturing and resistance aspects. To obtain resistance requisites, a new design has been offered; in this new design aluminum narrow bars are replaced by aluminum profiles which are mounted from inside of cases.At first, manufacturing aluminum profiles as a frame is thought to be more durable. Also, it emerged that welding would be more durable in comparison with screwing. Figure 2.18 shows this frame as a part of drawer case body.

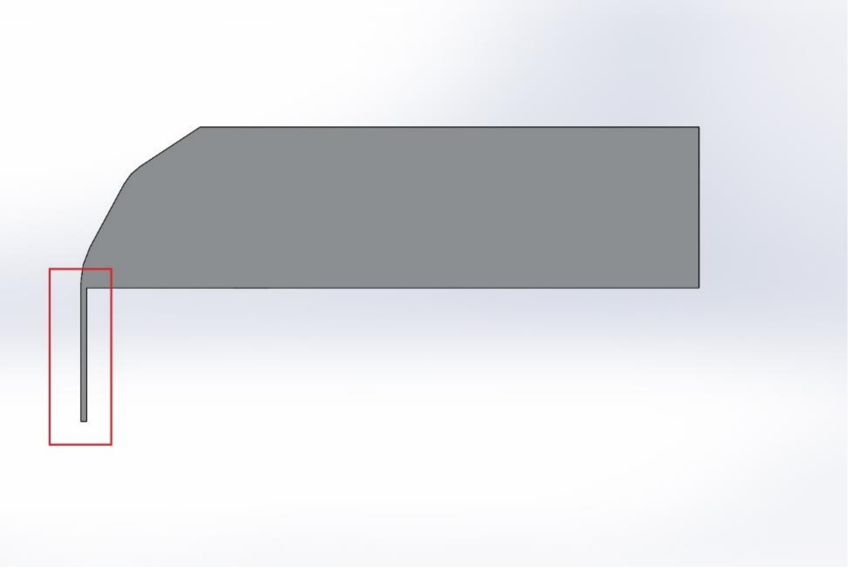

Figure 2.16 : Jet part attached to air guide.

Figure 2.17 : Sliding screw holes at the bottom surface of air guide.

It is suggested to use welding as aluminum profiles connection and screwing as their connection with exterior plates and parts.

Also, to accomplish screw elimination process at front plate, it should be welded to brackets from the inside of drawer case.

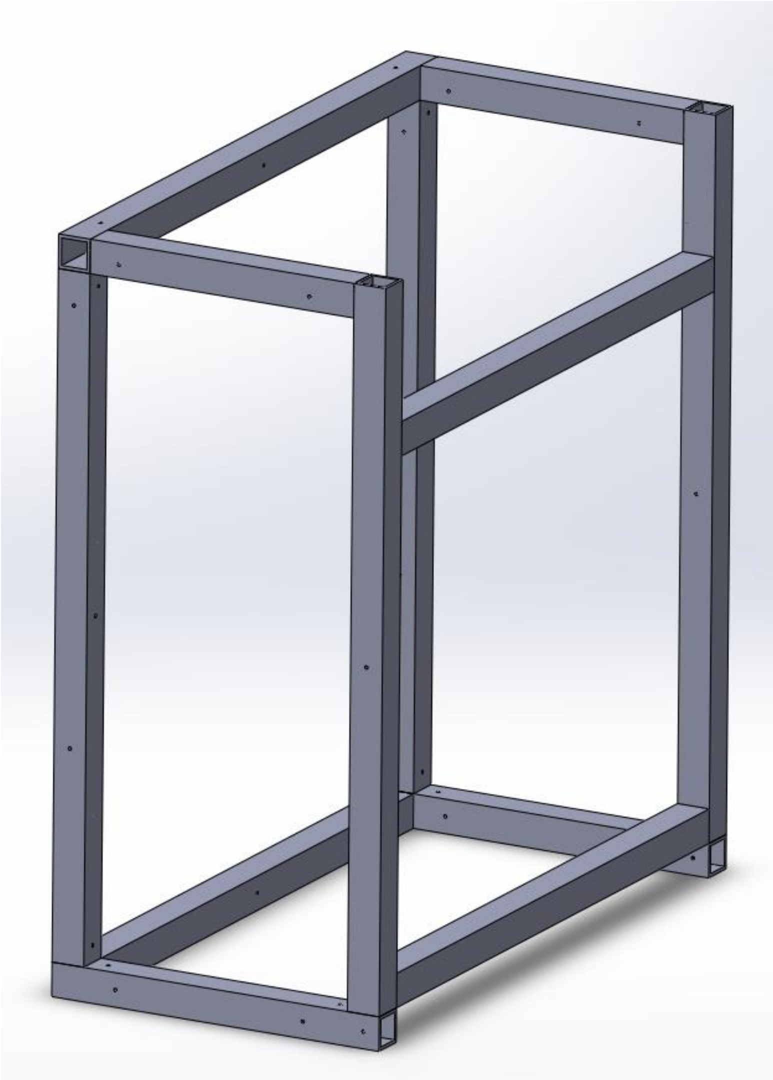

Figure 2.18 : Frame made with aluminum profiles.

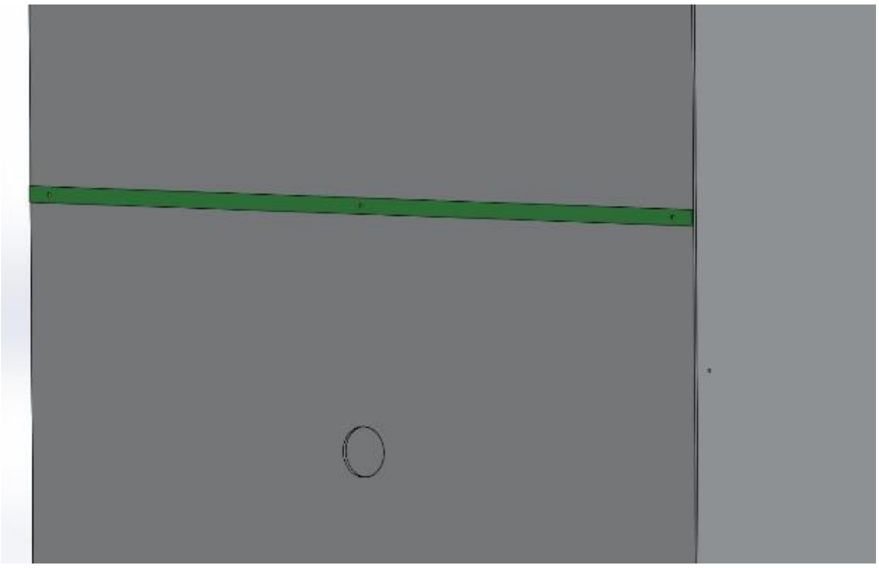

Figure 2.19 : A narrow aluminum bar is mounted on rear plate.

Finally, second design is given as seen in figure 2-20.

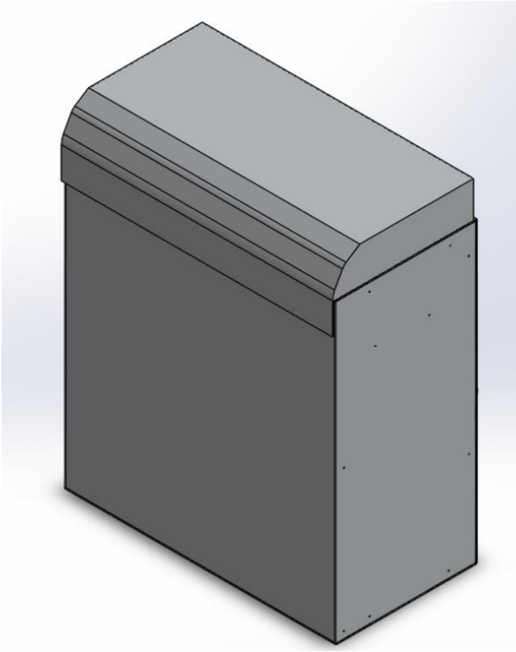

Figure 2.20 : Completed second design.

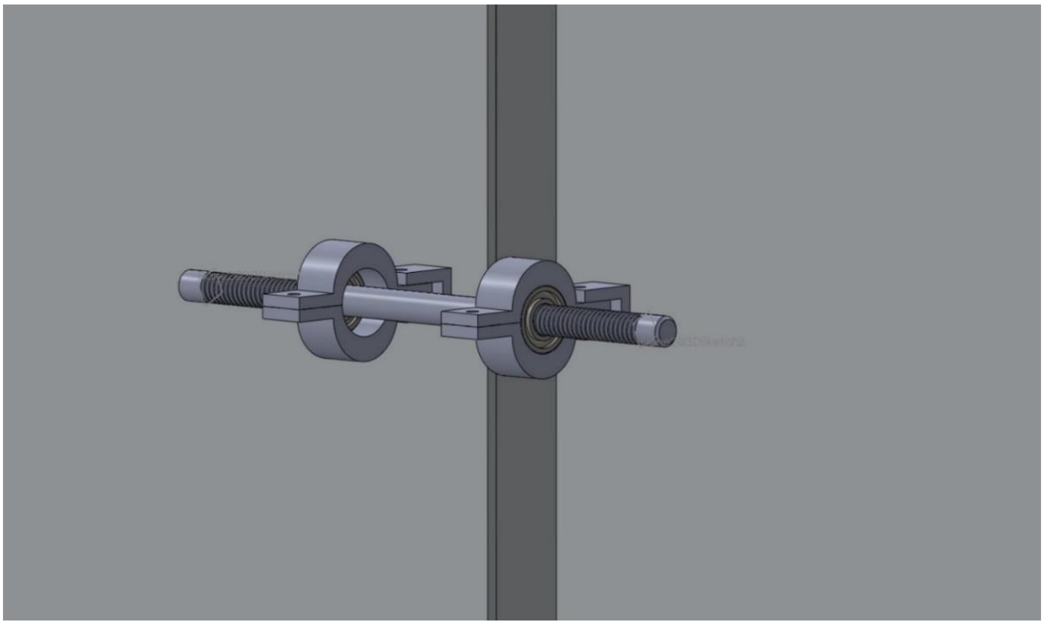

Figure 2.21 : Movement using a threaded rod.

It should be mentioned again that drawer is formed by two of this units shown on figure 2-20. Their distance should be adjustable during spun-bonding process; so these cases are linked to each other using a threaded rod, which makes possible to adjust mentioned distance by turning (Figure 2.21).

This threaded rod provides desired movement by attaching from both sides.

The distance between two attenuators should be closed during the process. Suggested solution to solve this issue, is to use elastic rubbers at both sides. It wouldn't just solve impermeability problems, but will provide an ability to yawn during the distance adjustment between two units.

There would be another problem about drawer movement at horizontal direction; they might lock when two drawer are moved by rod turning related to each other. To solve this problem 4 rods are mounted on all corners of drawer units (Figure 2.22). The mechanism which is used to connect threaded rod, will be used for corner rods too; but bearings will be used instead of nuts (Figure 2.23).

2.2 Cage Design

While two cases are moving related to each other, they should have the ability to move vertically in order to approach to die and get away from it especially at spun-bond process time. This movement ensures fibers uniformity at entrance section of drawers.

This function will be done by mounting two cases on a cage, which is formed by four vertical pillars supporting cases from four different points (Figure 2-24).

Figure 2.22 : Rods used on cases.

Cases will be mounted on pillars using the same rods which are used to prevent locking during the process; this will forestall more weights and holes on attenuator units (Figure 2.25). Bearings will be used to fasten pillars to drawer units too. Cases should have the ability of vertical moving of more than 1.5 meters and fastened up again at desired altitude; also its least altitude should be more than 0.5 meters as conveyor will be placed under the attenuator.

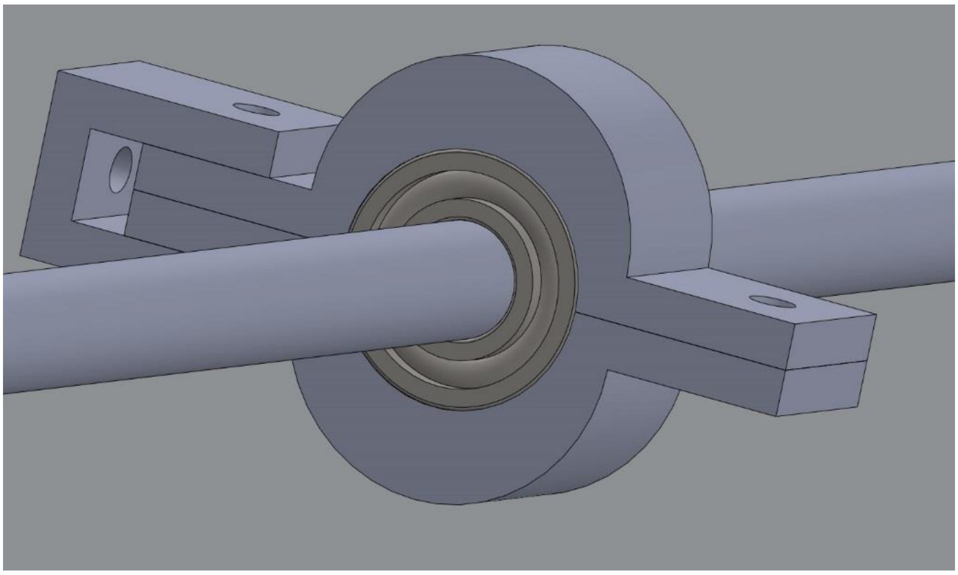

Figure 2.23 : Bearings used in rods.

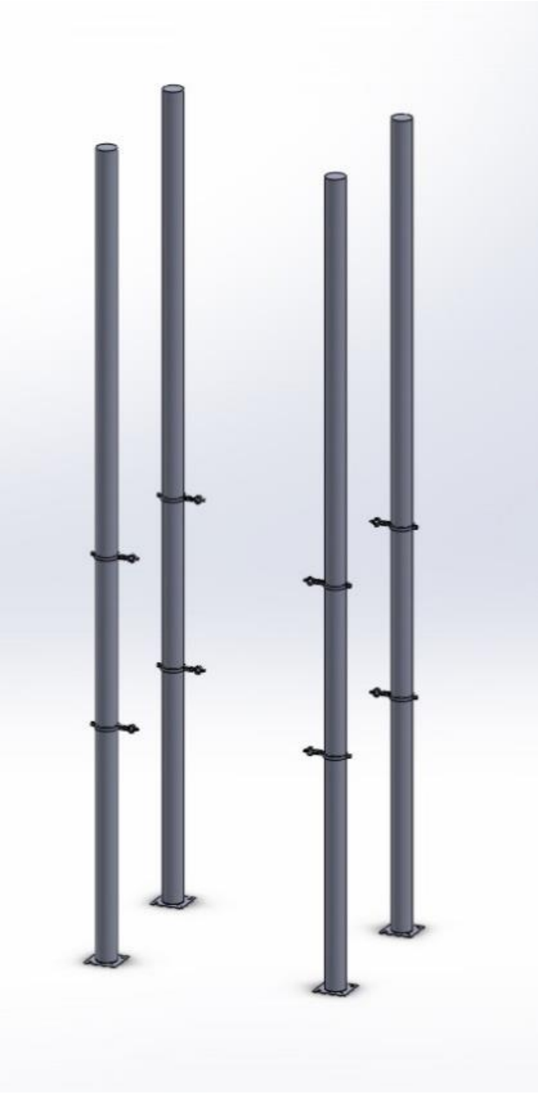

Figure 2.24 : Cage pillars.

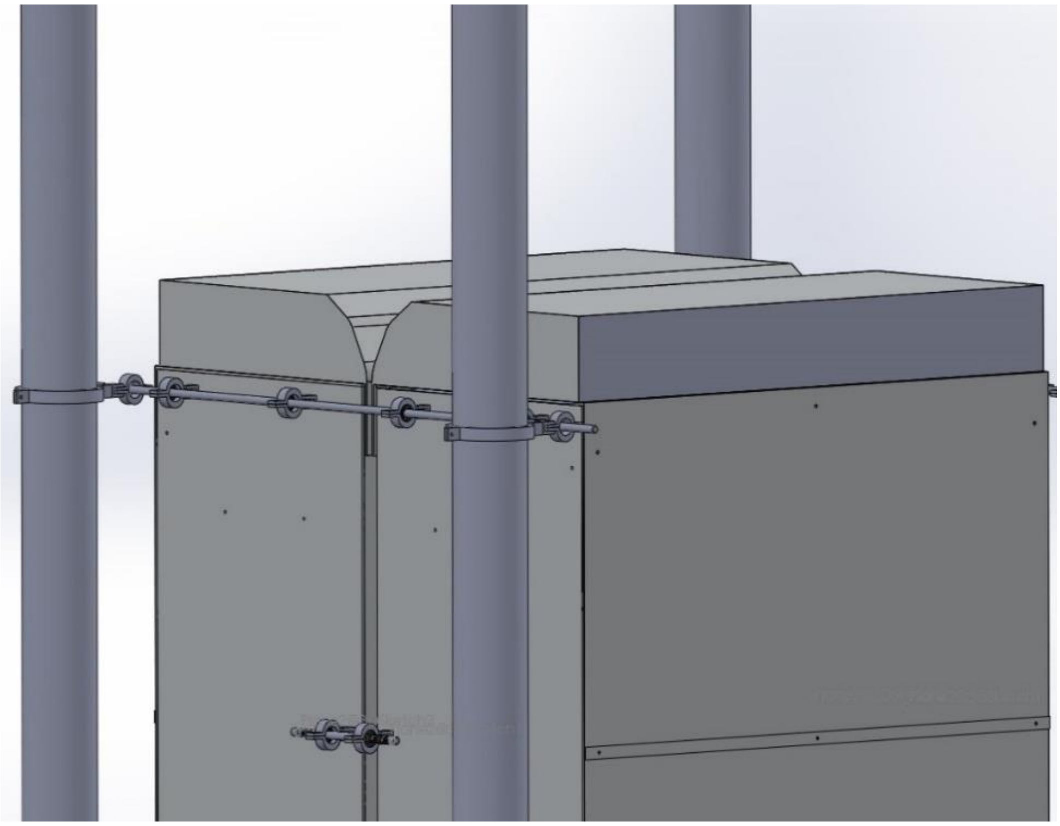

Figure 2.25 : Cases will be mounted on pillars using rods.

As shown in Figure 2.26 claps will be used to adjust altitude; in order to do this claps should be fastened up at desired place. Design has been turned out as shown in Figure 2.27.

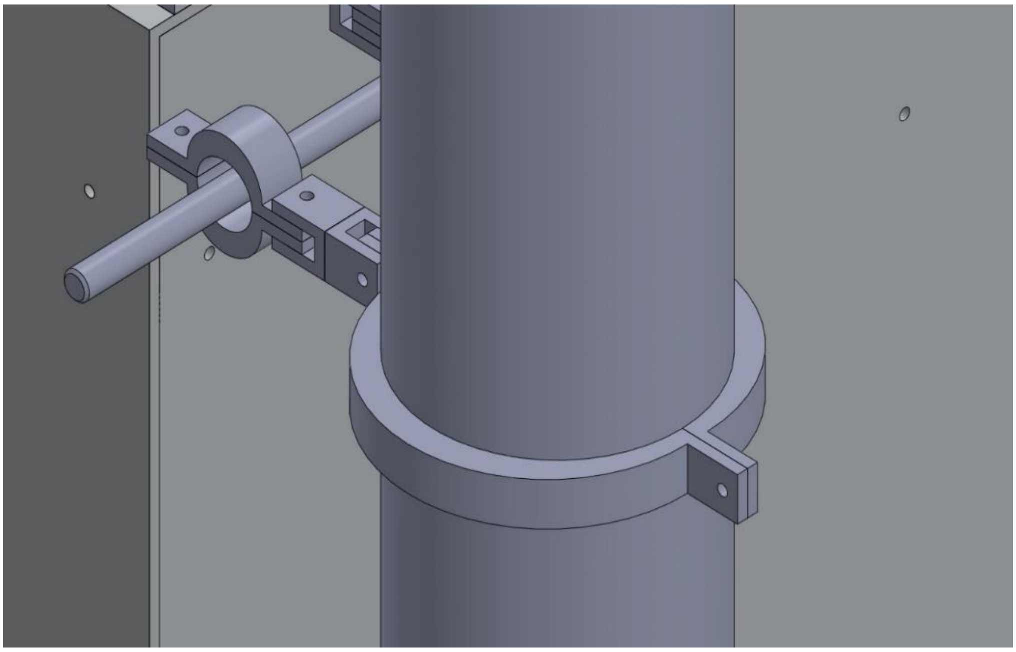

Figure 2.26 : Claps used on cage.

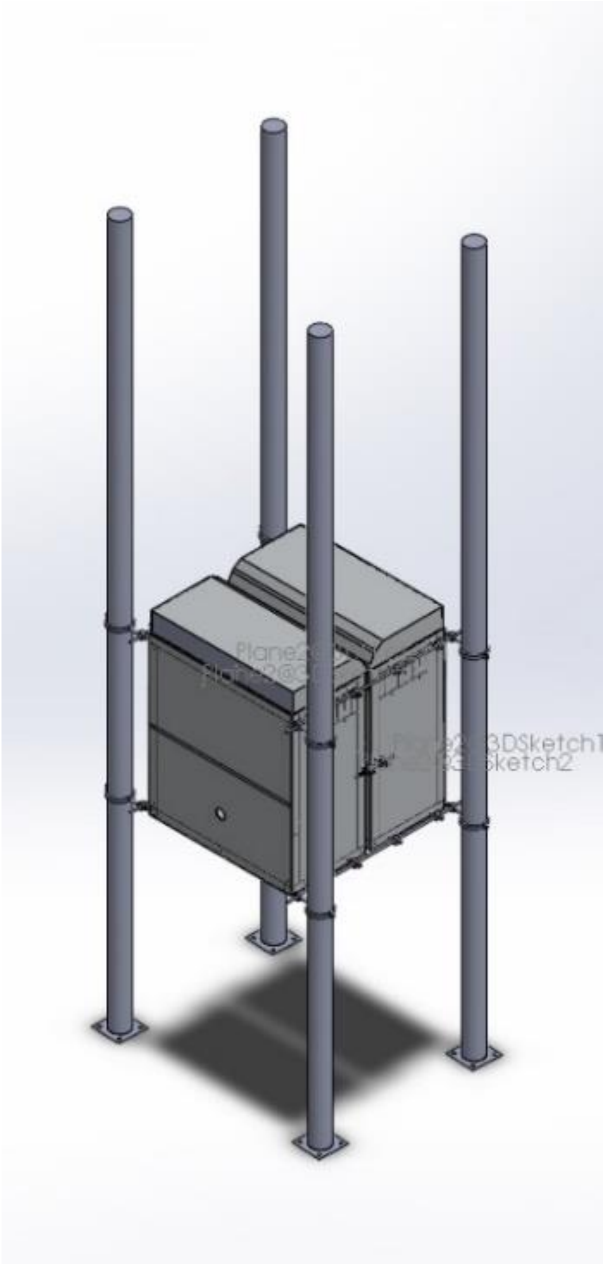

Figure 2.27 : Final condition of design.

2.3 CFD Analysis

Final design has been analyzed by CFD methods to ensure about fluid directions and appropriateness. It has been meshed using ICEM CFD and analyzed through FLUENT program; both are from ANSYS programs family. These programs and their solution methods are explained at “Computational Fluid Dynamics (CFD) Strategy” section.

As velocity is at high levels near the je section, there will be severe turbulence; in order to consider effects of turbulence flow k-ε model has been used during analysis. It adds Turbulence terms to Navier-Stokes equation.

2.3.1 Meshing stage

Desired mesh has been created by ICEM CFD program. Mesh could be created using automatic meshing method; but as a matter of fact, it doesn't have the ability of complex geometry identification as well as entrance and exit sections.

More mesh components are needed at sensitive and narrow sections in order to obtain more accurate results. Mesh components number is based on a variety of factors such as frequencies of turbulence vortexes, flow speed, exploited equations, etc.

Automatic meshing isn't able to create high mesh quality as same as which is created by manual meshing, even by a sensitive adjustment. Considering this fact results in exploiting manual meshing at sections with high velocity, more turbulence vortexes and narrow passages in order to form more finite volume elements.

First design is shown in Figure 2.28. In a normal solution 10-14 million meshes is used to solve this type of geometry. These numbers affects solution time severely. In order to decrease ram usage and subsequently solution time, one side of geometry has been meshed and symmetric solution has been utilized.

A pipe with a length of 0.5 meters has been used as entrance section. This long pipe provides enough space for flow to become developed. In order to obtain the finest mesh in this section, O-Grid meshing method has been used (Figure 2.29). This method eliminates triangular cells which results in fatal errors near pipe wall.

The rest of geometry has been meshed by considering wall effects and y-plus values. These conditions will guaranty the most accurate results and least deviation.

There are four millions finite volume elements at calculation field. The same methods used to mesh the second design. In order to consider all flow variables and air behavior inside cases, both sides of attenuator unit have been meshed and prepared for analysis. Again here O-Grid structure has been used in pipes; and wall effects have been probed during the meshing process. This mesh is shown in Figure 2.30. As shown here, mesh has a very smooth and uniform condition which makes it available to do analysis in less time.

As seen in Figure 2.30 number of elements increases by approaching to walls and vice versa. This geometry contains 8 millions of finite volume elements.

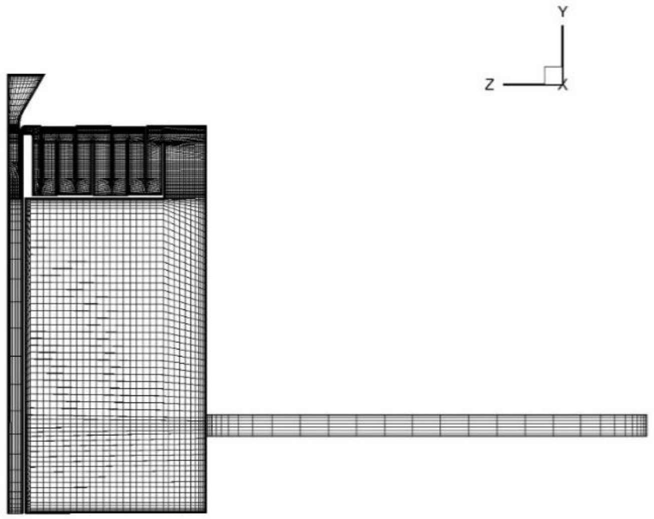

Figure 2.28 : Solution mesh structure of first design.

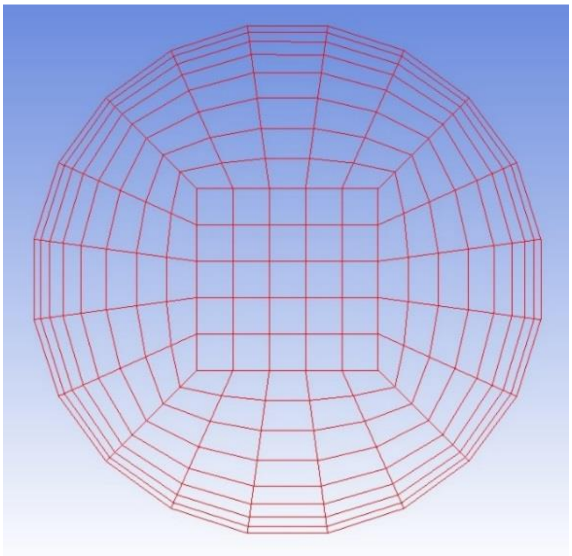

Figure 2.29 : Mesh structure inside pipes.

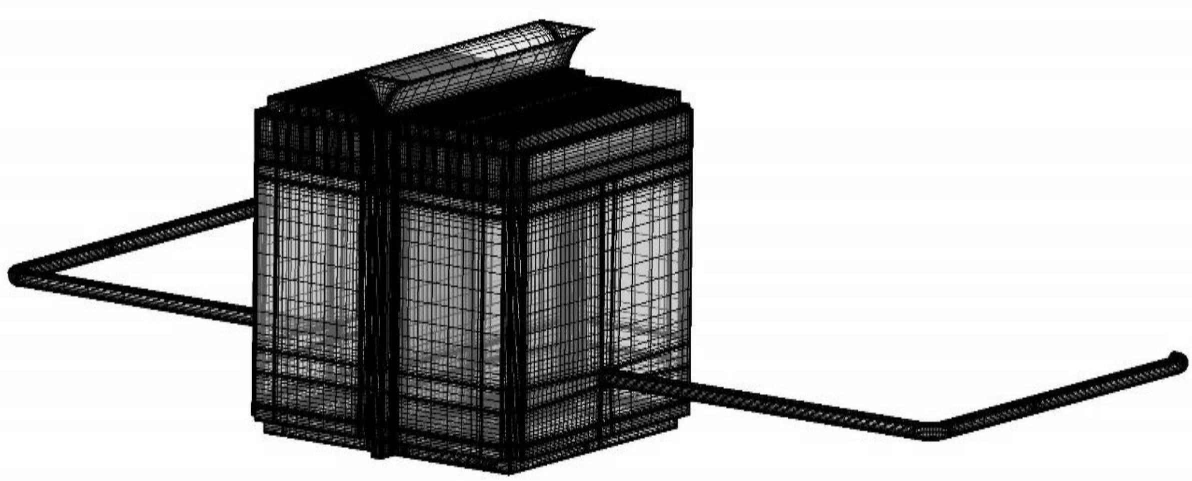

Figure 2.30 : Mesh structure of second design.

2.3.2 Calculations and results

Air entrance has been set to mass-flow inlet with an amount of 0.0864 kg/s. Exit and fiber entrance sections has the conditions of atmospheric pressure. They have been set to pressure-outlet boundary condition during solution (Figure 2.31).

Figure 2.32 shows velocity contours at a mid-section. Results shows a 135 m/s speed at jet section, which is a desired amount there.

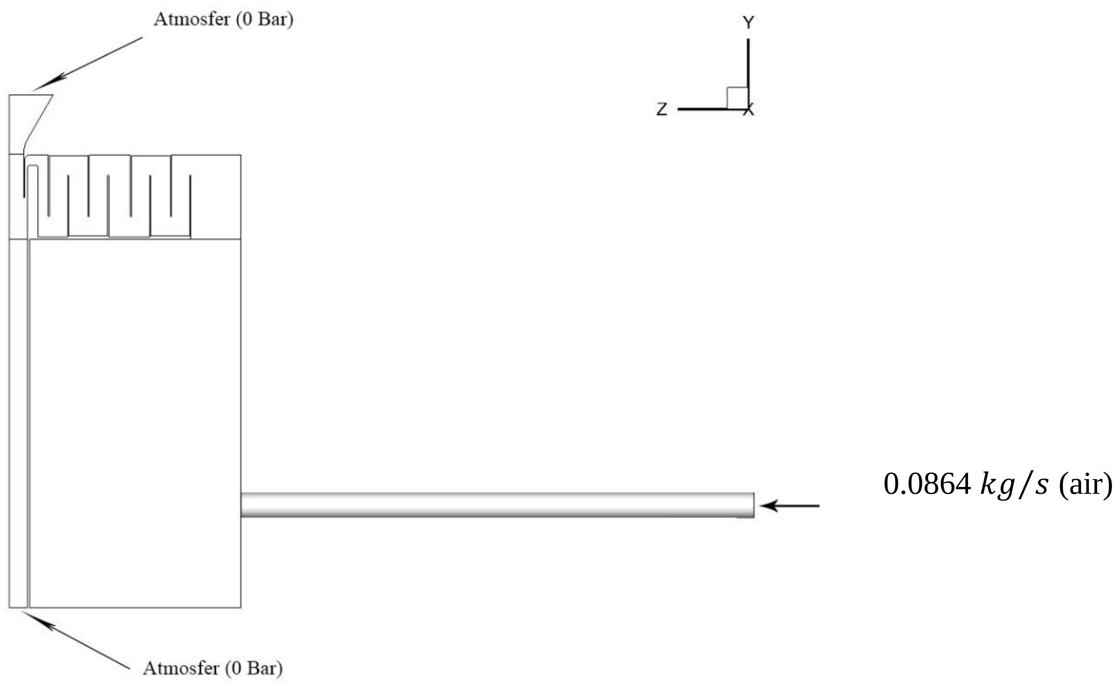

Figure 2.31 : Inlet and outlet values.

There is a vacuum formation at fibers cross section which is an intended result there; this vacuum will suck more air from fiber entrance section at the top of the attenuator. Pressure contour at drawer unit is shown in Figure 2.33. As shown in figure, the highest pressure is on the wall next to air inlet and the least pressure is at vacuum section.

Figure 2.34 shows air movement directions as well as vortexes a mid-section. As seen here, air reaches to jet section passing through narrow passages as had been intended during the design stage.

Figure 2.35 shows a mid-section at fibers movement filed. As is obvious, air velocity has a good uniformity at the whole width of mentioned section; this will result in an identical fiber flow throughout the interval.

Figure 2.36 shows pressure contours at the same mid-section. The same results of uniformity is seen for pressure throughout the interval width.

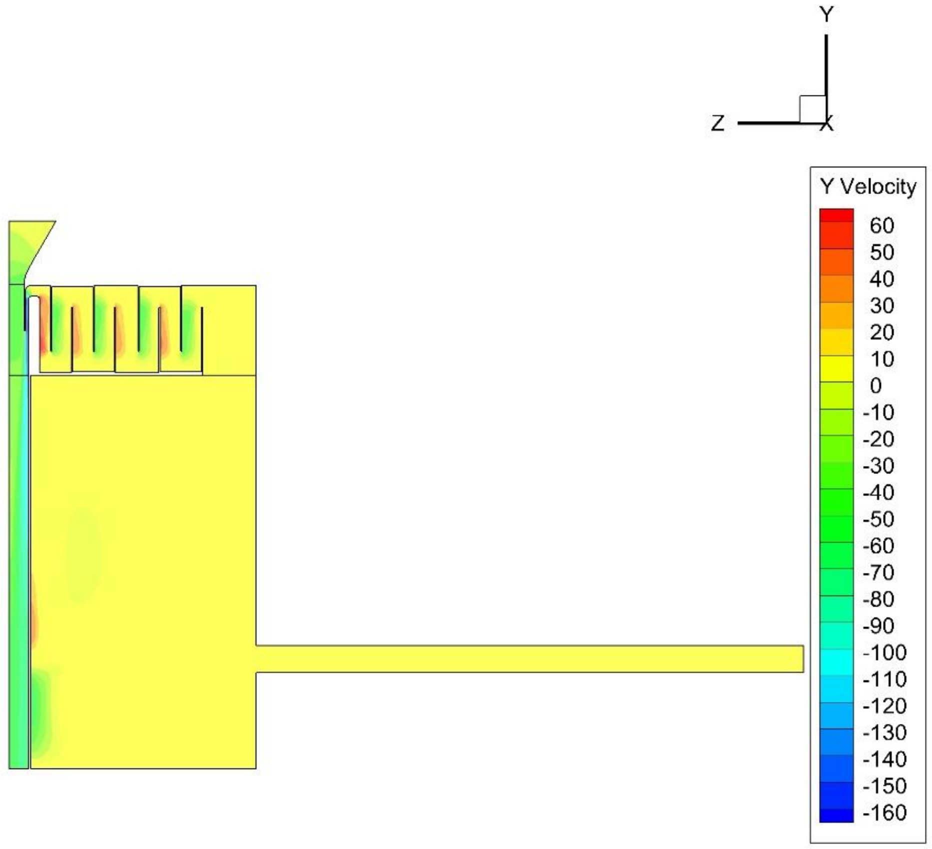

Figure 2.32 : Velocity contour of first design at a mid-section.

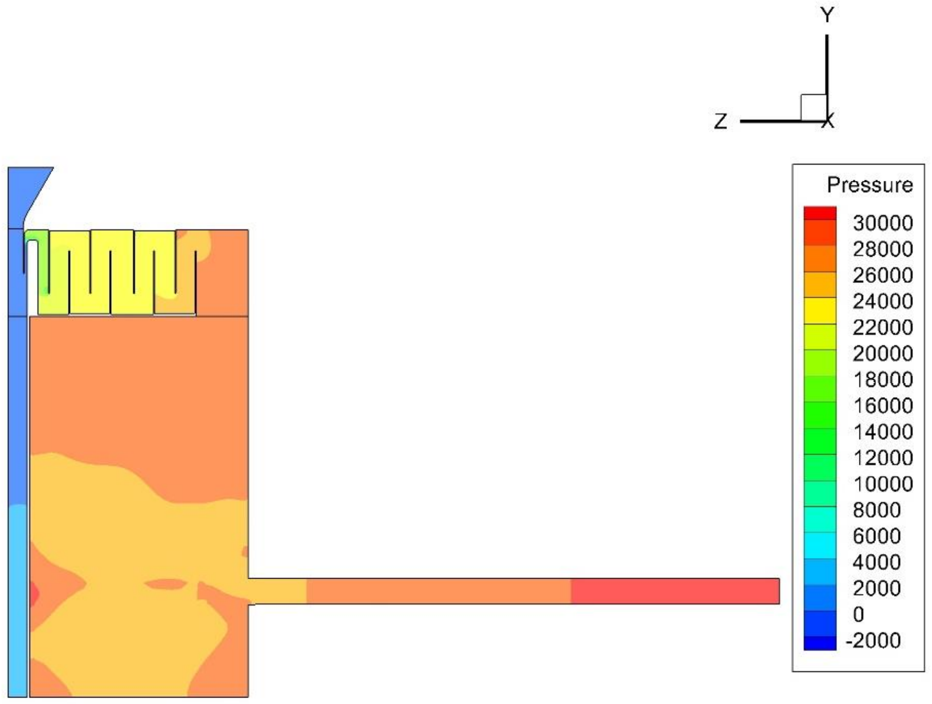

Figure 2.33 : Pressure contour at the same mid-section.

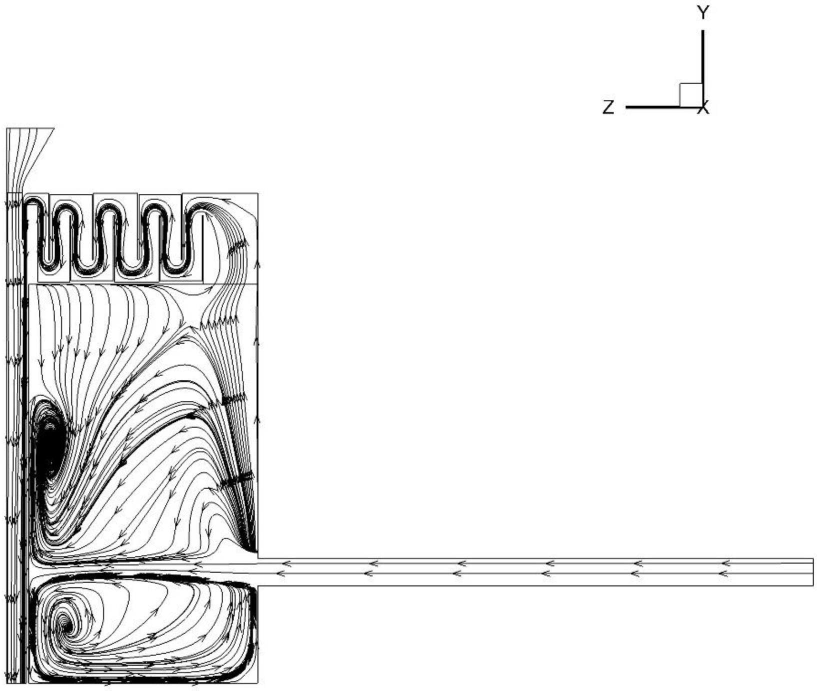

Figure 2.34 : Air movement directions and vortexes at the same mid-section.

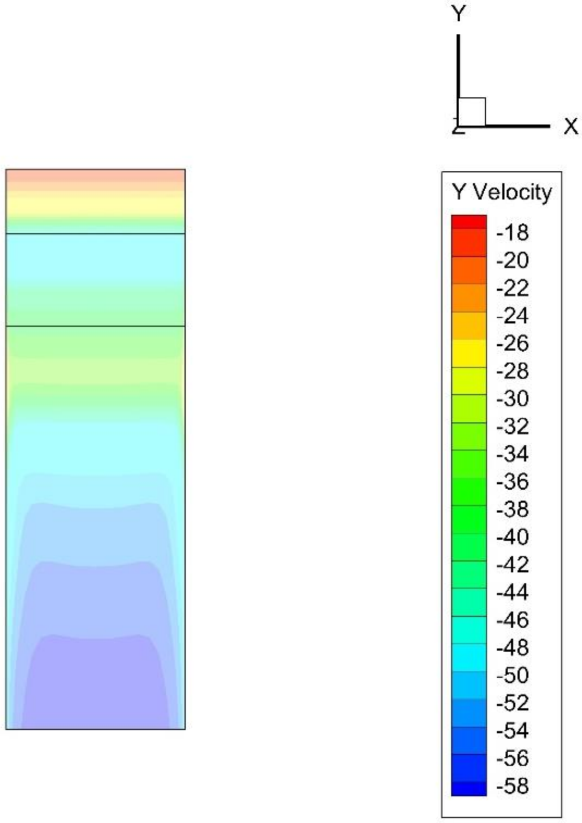

Figure 2.35 : Velocity contours at a mid-section of fiber passage.

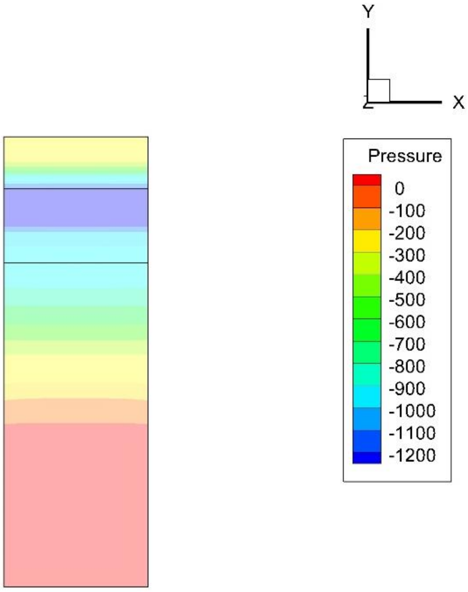

Figure 2.36 : Pressure contours at a mid-section of fiber passage.

Because of aluminum installment at interior part of drawers, there is less space for air there; as a results of this and to consider sharp corners of profiles effects on the flow, other calculations have been done on the second design too. Calculations have been done for the whole unit without using any symmetry surface. Input parameters are 0.0864 kg/s for each drawer.

Figure 2.37 shows CFD calculation results for Y-Velocity at a mid-section. There is a 5 m/s velocity decrement at jet section, which is 130 m/s. Since this decrement is not above the desired limit, it hasn't been considered as a major problem.

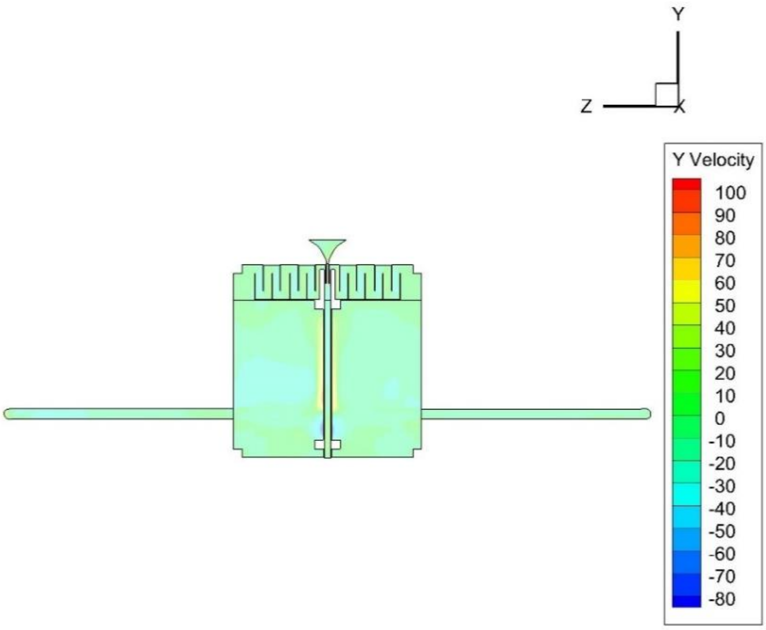

Figure 2.37 : Y-Velocity contours of second design at mid-section.

Pressure contours for the same section are shown in Figure 2.38; the same results as first design are seen in this figure for second one, which shows maximum pressure on the plate next to inlet gap, where air hits the wall and minimum one in vacuum section near jet.

Finally both results for first and second designs have been probed; both of them have close results for pressure and velocity which provide desired conditions as well. However, since second design is more durable and has a good resistance against vibrations, it is selected as the best and prepared for manufacturing.

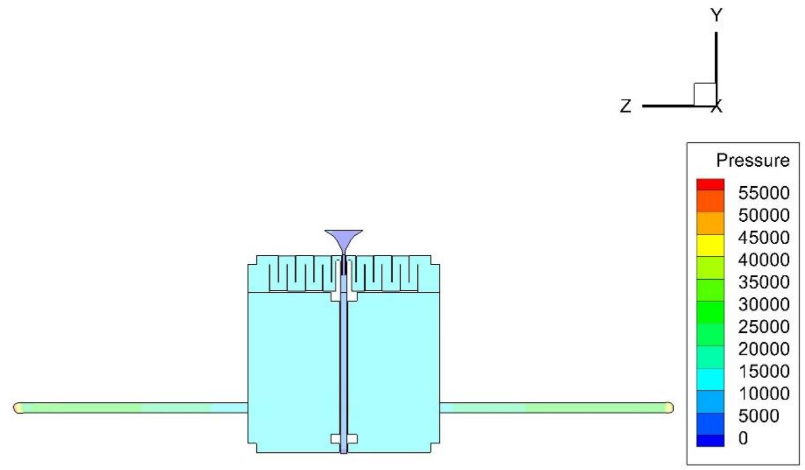

Figure 2.38 : Pressure contours of second design at a mid-section.

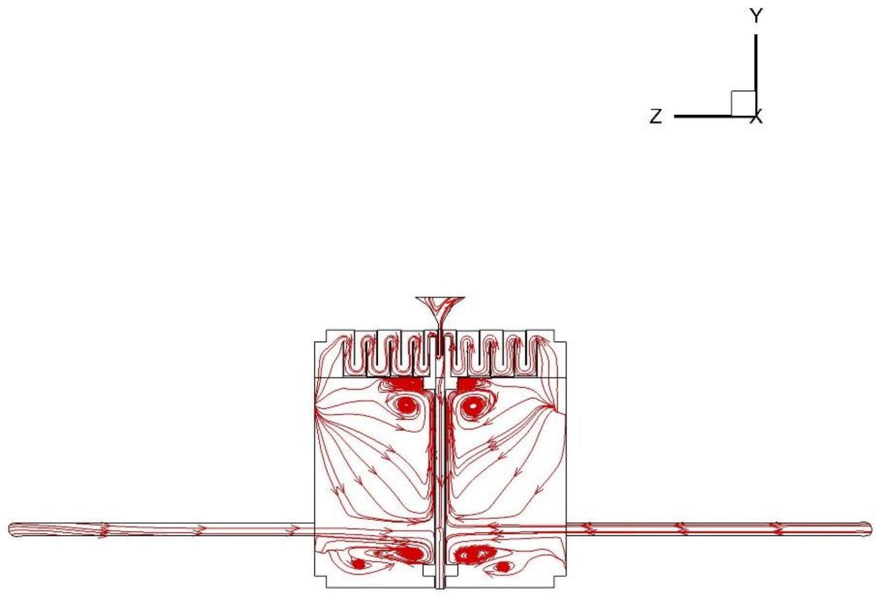

Figure 2.39 : Air velocity directions and emerged vortexes of second design at a mid-section.

3. MANUFACTURING PHASE

Minor changes should be done on design, even if design stage was done in a rigorous way. Formerly in this section, manufacturing of attenuator cases will be discussed; and later new extruder properties, which has been bought in the sake of spun-bonding process will be included.

3.1 Case Frame Manufacturing

As mentioned in design and CFD analysis section, second design, which includes frame and aluminum profiles, will be used in manufacturing process. In this process, aluminum frame will be considered for manufacturing at first steps. Frame will be manufactured using aluminum profiles, which will form it by welding.

Figure 3.1 shows welded frame; aluminum profiles are connected using aluminum weld. Some minor changes have been done in this step. Two profiles have been added to both sides (Figure 3.2); also front horizontal profiles have been realigned in the sake of more durability (Figure 3.3).

Figure 3.1 : Frame.

Figure 3.2 : Side profiles on frame.

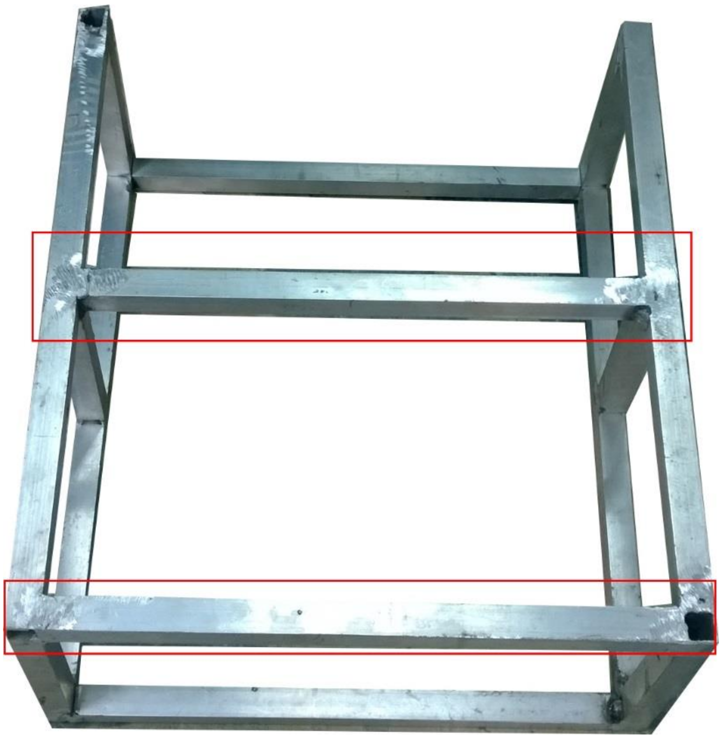

Figure 3.3 : Rearrangement on front horizontal profiles.

After this step, manufacturing continued focused on air channels. As mentioned at design section, these channels are used to increase air velocity; “L” shaped profiles have been used to form them. A “U” profile is formed using two “L” shaped one. Two achieve this goal, two “L” shaped profiles riveted on a plate next to each other. These channels are formed of two top and bottom faces. The former one is formed by riveting profiles on the bottom face of case cap and the latter one by riveting profiles on a plate. Finally four “U” channels, two from top and two from button, provide the desired function. Figure 3.4 and Figure 3.5 show bottom channels, which are formed using eight “L” or four “U” profiles riveted on a plate; this unit will be screwed to the front plate in a state which will not interfere with the passing fibers.

Figure 3.4 : Bottom channels.

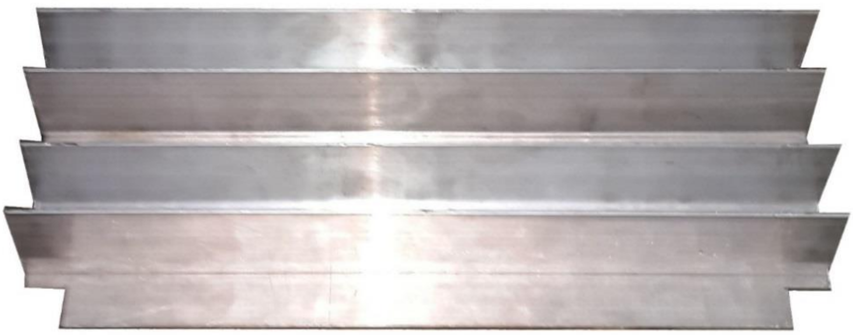

Figure 3.5 : Bottom channels.

Top channels are manufactured using the same techniques and materials; but it wasn't possible to mount the case cap after attaching the "U" channels; so they were attached while the cap was mounted on the case. Figure 3.6 and Figure 3.7 shows mentioned section.

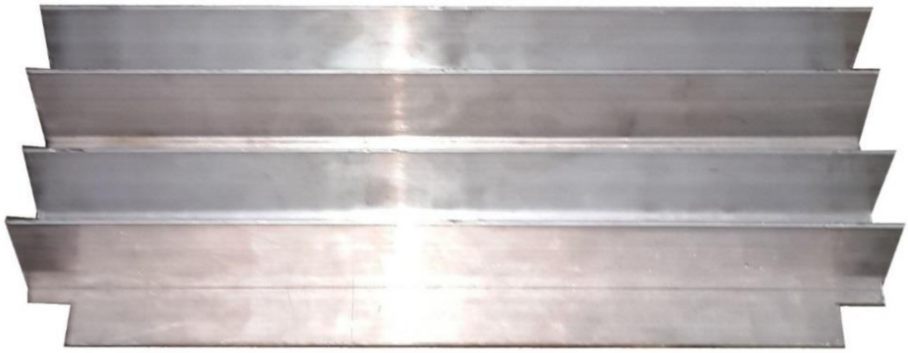

Figure 3.6 : Top channels.

Figure 3.7 : Top channels.

Unified state of channels is shown in Figure 3.8. As shown there, these channels are manufactured as same as what described at design section.

Air guide has been manufactured at next step. As described at design section, this unit will provide an effective sucking air condition from top of the attenuator. This unit has been manufactured by bending front part of a plate as an "S" and its sides by 90 degrees. Then, this plate has been attached by screwing on another plate and prepared for mounting on the case. Figure 3.9 shows air guide.

Figure 3.8 : Unified channels.

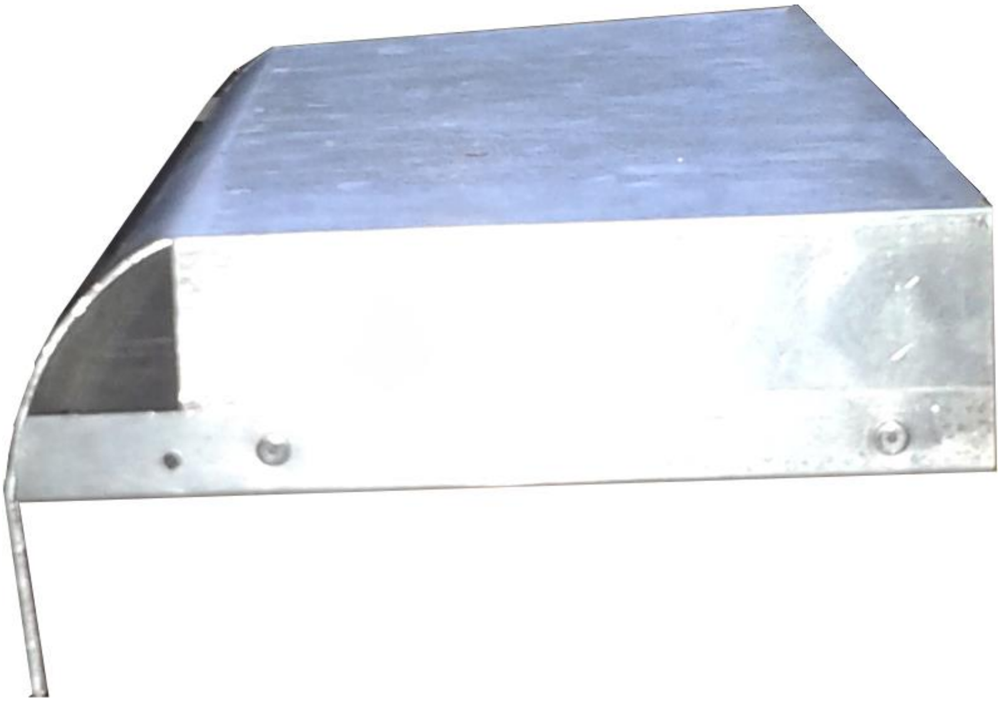

Figure 3.9 : Air guide.

Figure 3-10 shows the back plate; as discussed at design section, the pipe material is aluminum which has been attached to back plate using silicon clue.

Finally, all parts have been unified using screws and formed the attenuator case. Figure 3-11 shows final case.

As a final result, drawer has been manufactured and made ready for operation.

Figure 3.10 : Drawer case.

4. RESULTS VALIDATION OF SECOND DESIGN

Drawer design is based on a variety of variables such as blower power, air corridor gap between two drawers, jet gap width, etc. This unit has been tightened using different methods against air leak; and in the sake of an experiment has been tested using a fan which had a power of 7.5 kW and a pressure of 0.07 bar. Figure 4.1 and Figure 4.2 show the fan and mounted drawer case on it. Since this unit has been selected as a test, the case has been mounted on the fan horizontally.

Figure 4.1 : The fan and mounted drawer case on it.

Figure 4.2 : The fan and mounted drawer case on it.

The fan properties are shown in Table 4.1.

Table 4.1 : Testing fan properties.

Power (kW)	Pressure (Pa)	Flow rate (m^3/h)
7,5	7100	4000

Tests have been done pressure based using a 3 mm of jet gap. Velocity has been measured using a pitot tube at the exit section.

Also a CFD analysis has been done related to this condition and results have been compared. CFD results are shown in Figure 4.3 and Figure 4.4 for a jet gap of 3 mm and inlet pressure of 0.07 bar. To attain a realistic validation two sides of the drawer have been considered as open gaps as like as what has happened during the experiment. Results of CFD analysis are shown in Table 4.2 and compared with experimental results.

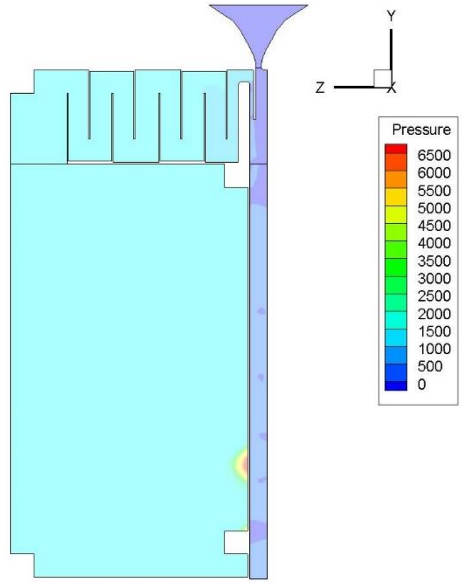

Figure 4.3 : CFD pressure results in test conditions.

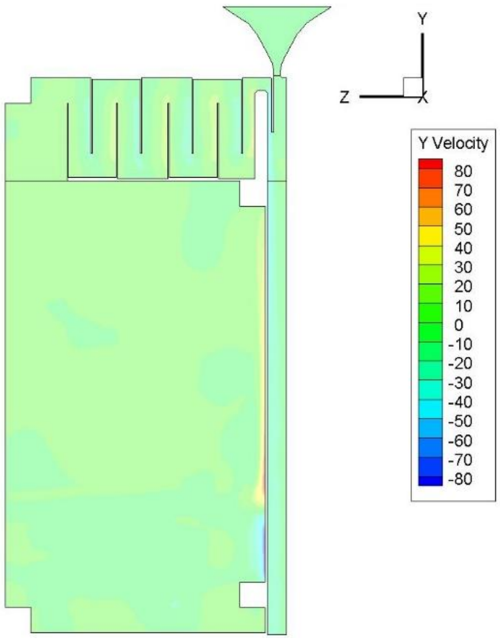

Figure 4.4 : CFD velocity results in test conditions.

Table 4.2 : Comparing CFD and experimental results.

Condition	Jet speed (m/s)
Experiment	34
CFD	31

As seen, CFD and experimental results are in a good coincidence and deviation is 8%. These results supports CFD analysis accuracy and let us optimize the design by trusting CFD results.

4.1 Confronted Problems in Second Design and Solution Tips

Some problems have emerged at experimental stage as followings:

1. Since these experiments were done just as tests, exploited fan didn't carry desired properties; a fan, which is capable of providing desired speed, should be able to produce a pressure of 0.55 bar; where exploited fan was capable to produce 0.07 bar. Considering the fan size leads us to recognize desired fan size which will be very large.
2. Another problem which was confronted at experimental stage was tightness against air leak. Since aluminum was selected as the material to reduce weight, it was impossible to use welding on side plates of the attenuator cases. So it was concluded in attaching plates to profiles using glues. Experimental results shows air leak at different points even at low pressures. When the operation commenced, air started to leak from corners and cap part of the case.
3. Finally, because of air leakage at jet gap, its panel started to widen by adding more air pressure. This will decrease air velocity at jet section and consequently at fiber exit.

Problems which were confronted at experimental stage lead us to conclude in thinking of another simpler and more durable design in which pressure drop is lower.

5. DEVELOPMENT OF NEW DESIGN

Considering problems which were confronted at last section, two new designs have been put forth. The most important problem is about pressure drop; since it is just related to internal design of case, exterior parts such as body, drawer cage and jet section haven't been changed; so only interior part has been taken into account. Since the goal is to obtain velocity using provided pressure, air cross section should be continue in a narrowing state. If air enters in a wider section, it loses its velocity because of pressure drop; as a result, the pressure which spent to accelerate will be wasted. So air should not pass from a narrow passage to a wider one. This matter has been considered as an important one in two new designs. Then, one of these two design has been selected and CFD analysis have been done and compared on it. CFD analysis have been done in both desired velocities and test fan properties. After, to eliminate problems some change have been done on selected design. Finally, practical drawings have been prepared and the case manufactured.

To eliminate jet plate bending problem, some material researches have been done; finally stainless steel has been selected as appropriate one. By this, the problem which was because of aluminum usage as material has been eliminated.

Also some researches have been done on tightness matter and the best practical method has been selected; to conquer this problem, it is decided to use stainless steel as internal sections material and weld them o two sides' plates. In this way, by the best and economically cheapest method the tightness issue will be resolved.

5.1 Third Design

Firstly, to decrease pressure drop, air channels converted to vertical passages which are narrowing through the air passage. Figure 5.1 shows third design air channels.

As shown in Figure 5.1, at every section air partitions are getting closer to front and rear plates as well as to each other. In this way, air is gone through a narrower space at each section and it will no longer enter from a narrower to wider area.

Mentioned design hasn't been selected as an appropriate one because of manufacturing and vibration problems.

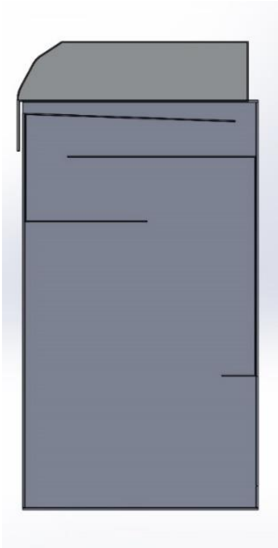

Figure 5.1 : Third design air channels.

5.2 Forth Design

Forth design has been planned in a way which will carry desired features and eliminate previously encontoured problems. This design has been optimized and after some stages has been arranged to the best way.

Firstly, fiber drawing system has been represented as Figure 5.2. As seen in Figure 5.2, as a matter of pressure drop decrement, air channels were prolonged and narrowed through the passage.

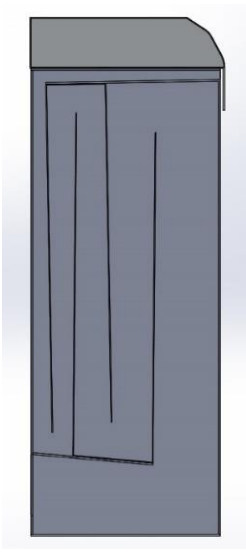

Figure 5.2 : Forth design primitive representation.

Furthermore, partitions have been designed with slight angles and attached to side plates; so air tunnel is narrowed through its way to jet. Because of manufacturing issues this representation has been changed and partitions' angles have been eliminated.

Entrance section of forth design is shown in Figure 5.3. In the sake of preventing pressure drop at pipe which connects fan to drawer, the entrance has been enlarged to an amount which has been discovered by doing different researches on variety of fans.

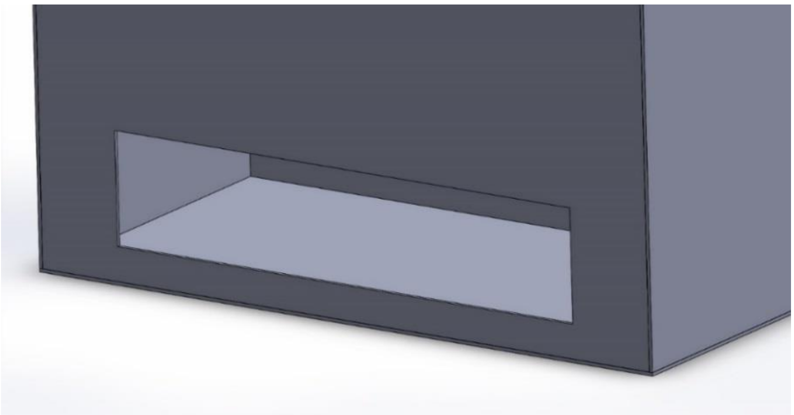

Figure 5.3 : Forth design entrance section.

The cap of drawer has been designed as the first representation and to prevent jet plate blending, material which has been used for its manufacturing, changed to stainless steel. This part, which is shown in Figure 5.4, has the functionality of jet exit plate as well as air guiding.

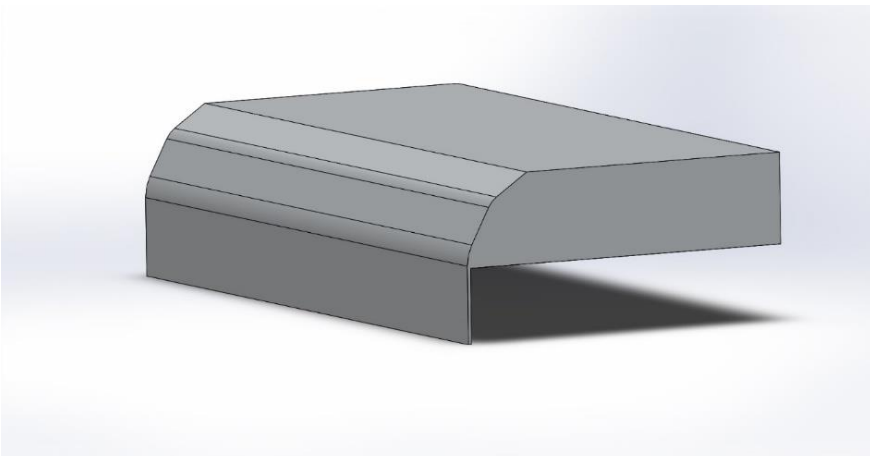

Figure 5.4 : Forth design drawer cap.

Figure 5.5 and Figure 5.6 show CFD results of this representation. In the sake of comparisons, entrance value has been selected as 0.2 kg/s as it was prior designs. Jet gap has been set to 3 mm and its velocities has been measured.

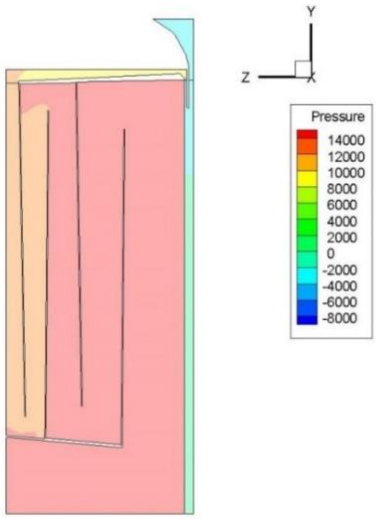

Figure 5.5 : Pressure contours for forth design primitive representation.

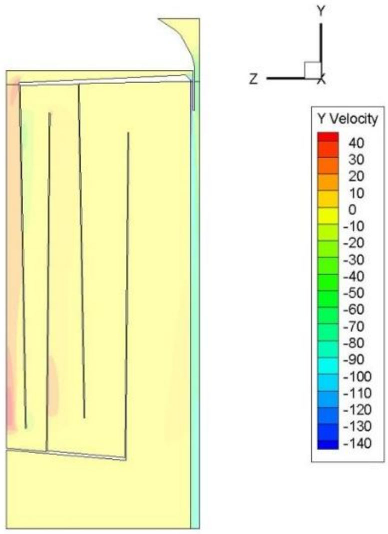

Figure 5.6: Velocity contour related to forth design primitive representation.

As seen in former figures, these designs provides less pressure drop (0.14 bar) and higher jet velocity (140 m/s) in comparison with prior designs.

Vertical movement of attenuator has a significant importance; this movement will provide the ability of grabbing fibers immediately at die exit during the start stage of production. To obtain this, drawers should as close as possible to die. Afterwards, drawers should be get far from the die to provide cooling and prolonging time for fibers. The elastic pipe which is shown in Figure 5.7 will provide the ability of this movement.

Drawer has a rectangular entrance, which will be connected to mentioned pipe using a designed apparatus. This apparatus is shown in Figure 5.8; thee negative effects of this apparatus and mentioned elastic pipe should be considered during calculations.

Figure 5.7 : The elastic metal supported pipe which will be used as drawer and fan connection.

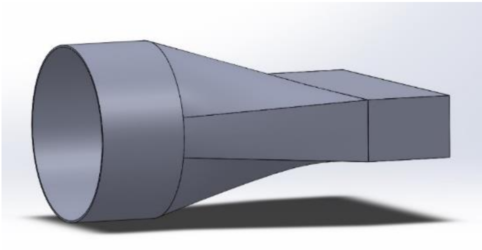

Figure 5.8 : Connection apparatus between drawer and elastic pipe.

As mentioned before, presented design should be slightly change to eliminate manufacturing problems; the most important one of this changes, is removing angles in all parts except jet entrance.

The CFD analysis results, which have been done on changed design, are shown in Figure 5.9 and Figure 5.10. As seen in results, eliminating plates' angles doesn't affect pressure drop and velocities excessively; therefore, it has been decided to manufacture channels plates without angles.

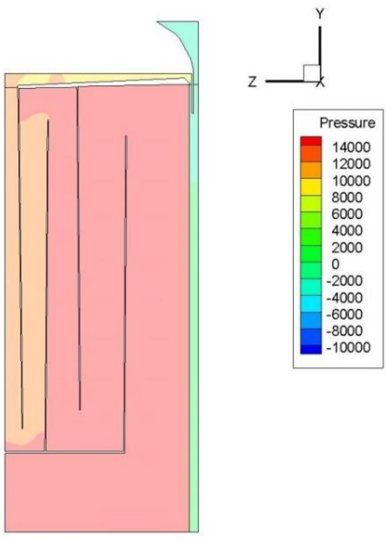

Figure 5.9 : Pressure contours for changed forth design.

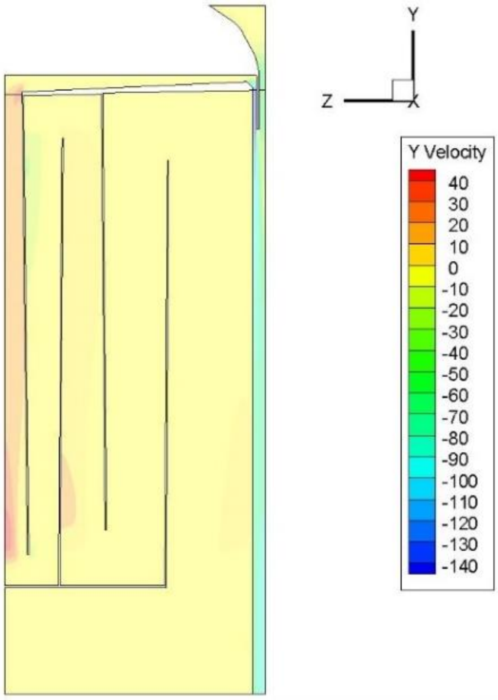

Figure 5.10 : Velocity contours for changed forth design.

As mentioned before, bending of jet gap plate is a major important; a solution in which jet gap plate is attached using five rods with a diameter of 1 mm to front plate has been suggested to solve this problem. CFD results related to this subject are shown in Figure 5.11.

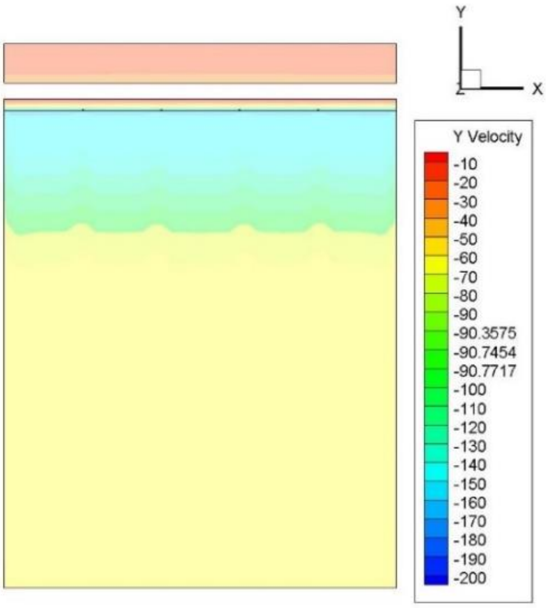

Figure 5.11 : The effects of rods at jet section.

As seen in Figure 5.11 these rods prevent uniform air distribution; as a result fibers would not advance at correct direction; therefore, instead of using rods, making the jet plate from a steel material has been preferred in the sake of durability.

Since a fan with high pressure and mass flux properties is very expensive and in the sake of preventing a wrong fan selection, CFD analysis have been with different jet and drawer gaps and different mass fluxes. At the same time, using these analysis, achieving more velocities have been probed. These analysis have been done for three mass fluxes of 0.2, 0.3 and 0.4 m^3/s and results are shown in Table 5.1. As is obvious in this table, more fluxes will cause in more pressure drops.

Table 5.1 : CFD analysis for 5 mm jet gap.

Flux	Drawer Gap	Jet Gap	Pressure Drop	Sucked Flux	Highest Velocity in Jet Section	Highest Velocity at Drawer Exit	Fan Power (kW)
0,2 kg/s	20 mm	3 mm	0,16 bar	0,13 kg/s	185 m/s	71 m/s	2,61
0,2 kg/s	40 mm	3 mm	0,18 bar	0,30 kg/s	187 m/s	53 m/s	2,93
0,3 kg/s	40 mm	3 mm	0,40 bar	0,44 kg/s	275 m/s	77 m/s	9,79
0,4 kg/s	40 mm	3 mm	0,70 bar	0.58 kg/s	384 m/s	102 m/s	22,85

Since sucked air from the top of attenuator, which is a result of formed vacuum near the jet, is an important factor, it has been included in Table 5.1. As seen above, opening the gap between two drawers besides of increasing sucked air from environment, will increase pressure drop too. But as an important matter during spun-bonding process, larger gaps should be considered as well.

Higher mass fluxes results in higher velocity and consequently thinner fibers. But pressure drop increment which is a result of higher fluxes shouldn't be omitted. As pressure drop increases to 0.4 bar in a mass flux of 0.3 kg/s and 0.7 bar in a mass flux of 0.4 kg/s, they have been considered as inappropriate inputs. Also, it is obvious that air velocity is less at 0.2 kg/s of mass flux and 40 mm of drawer gap. In this situation the best choice is 0.2 kg/s of mass flux and 20 mm of drawer gap.

Table 5.2 shows CFD analysis results for 5 mm jet gap. Since this gap size is only used for 40 mm drawer gap width, only the results for mentioned conditions are brought in mentioned table.

Pressure drop as a limiting characteristic, leads to a restriction which obliges a 0.3 kg/s of mass flux at 5 mm jet gap and 40 mm drawer gap size.

Since air velocity at exit section with a 0.2 kg/s of mass flux is well below of desired quantities, it is eliminated as an inappropriate condition. Therefore, only 0.3 kg/s of mass flux is the best situation for this combination.

Conclusively, suggested work conditions are brought in Table 5.3.

Table 5.2 : CFD analysis results for 5 mm jet gap.

Air mass flux	Drawer gap	Jet gap	Pressure drop	Sucked air	Highest air velocity at jet	Highest air velocity at exit	Fan Power (kW)
0,2 kg/s	40 mm	5 mm	0,07 bar	0,19 kg/s	82 m/s	40 m/s	1,14
0,3 kg/s	40 mm	5 mm	0,16 bar	0,28 kg/s	179 m/s	61 m/s	3,91
0,4 kg/s	40 mm	5 mm	0,30 bar	0,38 kg/s	238 m/s	81 m/s	9,79

Table 5.3 : Suggested gaps and mass flow rates.

Air mass flux	Drawer gap	Jet gap	Pressure drop	Sucked air	Highest air velocity at jet	Highest air velocity at exit	Fan Power (kW)
0,2 kg/s	20 mm	3 mm	0,16 bar	0,13 kg/s	185 m/s	71 m/s	2,61
0,3 kg/s	40 mm	5 mm	0,16 bar	0,28 kg/s	179 m/s	61 m/s	3,91

Therefore, a fan with 0.16 bar of pressure and 0.3 kg/s of mass flow rate should be able to provide desired conditions. Some researches has been done related to this result and an appropriate fan has been selected.

After selecting desired fan properties, some other CFD analysis have been taken into account including one which contains fibers. Boundary conditions for this analysis have been arranged using results taken from previous ones. As the problem related to internal part of drawers has been solved and also, by considering 374 fibers with a diameter of 0.3 mm effect on mesh aspect ratio and its number of cells, it is decided to take only the drawer gap section into account.

The results of this analysis are taken in Figure 5.12, Figure 5.13 and Figure 5.14; input parameter for this analysis is 130 m/s velocity input at jet, which is a result of previous analysis. Outlet boundary conditions are as same as before. Again meshing, which is used here, is structured mesh. The fibers are considered as solid materials which move with a speed of 20 m/s (as considered to be) upside down. As shown here, fibers don’t affect pressure and velocity significantly.

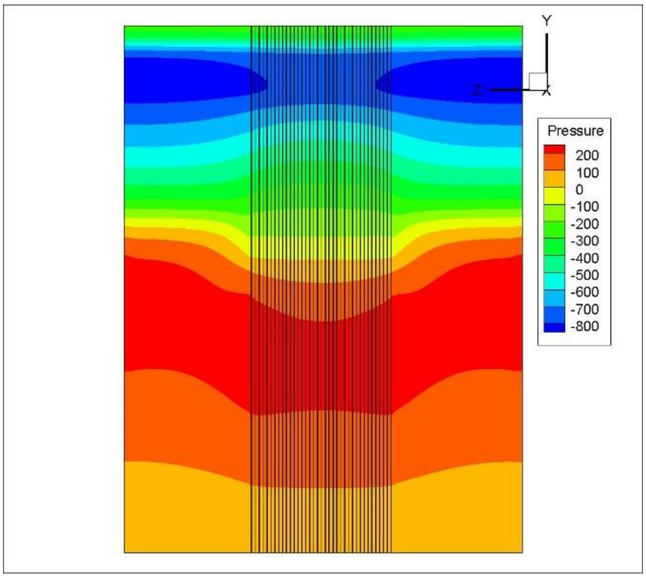

Figure 5.12 : Pressure contours of forth deisgn including fibers movement.

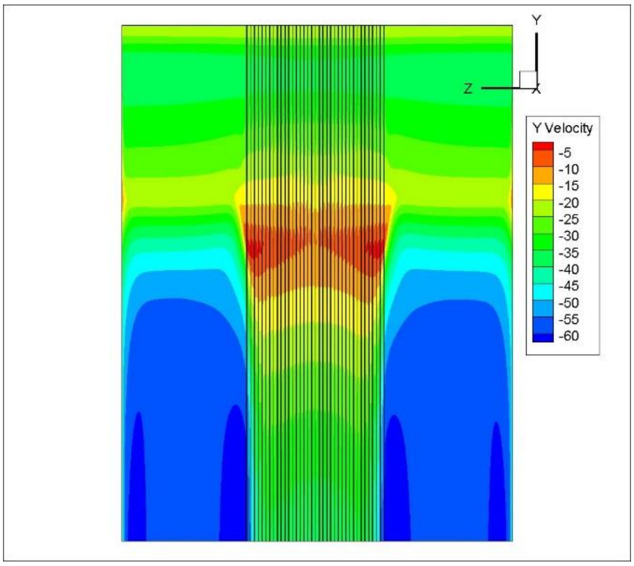

Figure 5.13 : Velocity contours of forth deisgn including fibers movement.

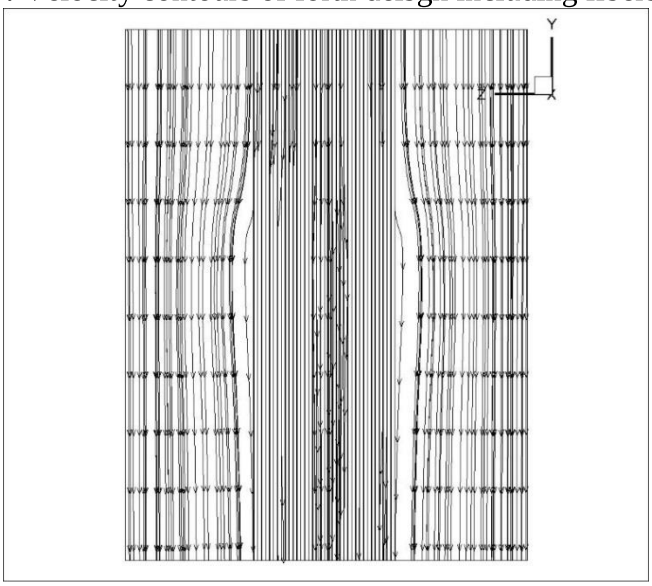

Figure 5.14 : Air directions of forth deisgn including fibers movement.

6. DRAWER MANUFACTURING

After finishing drawer design process, some changes have been done on it to consider restrictions of manufacturing facilities. Some changes, related to tightness and manufacturing, have been done at drawer internal section; these changes are shown in Figure 6.1.

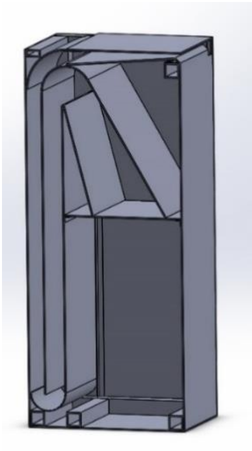

Figure 6.1 : Drawer design after modifications.

As seen here, air channels have been curved at transitions. This condition will ease air movement through the channel and consequently decrease pressure drop. Also, it is taken care to unify these partitions as much as possible. These partitions are shown in Figure 6.2 a, b, c.

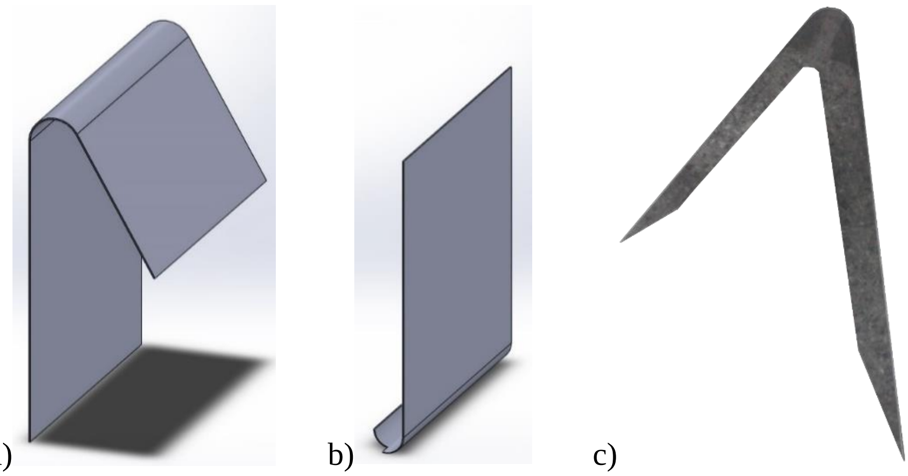

a) b) c)

Figure 6.2 : Air partitions.

Placing air input gaps on rear plate will increase the chance of touching conveyor by air pipes. To prevent this, air entrances have been moved to side walls; also their shapes changed to circle which will eliminate connection apparatus requirement. Figure 6-3 shows this modification.

Air should be guided to air partitions after entrance; to obtain this, an elbow with an angle of 90 degrees. A flange has been used to connect the elbow to air partitions. Figure 6.4 shows this elbow and its flange.

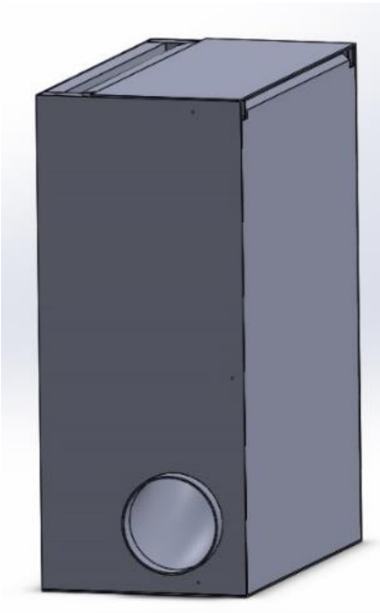

Figure 6.3 : Air entrance.

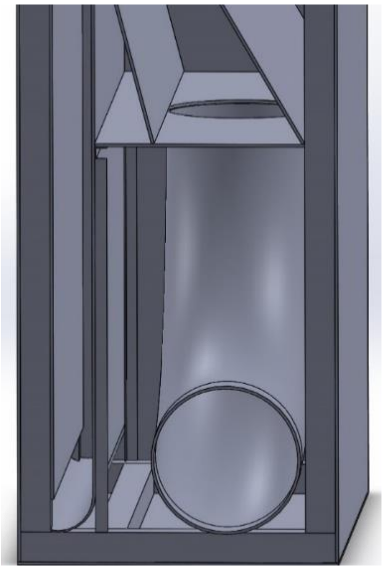

Figure 6.4 : Air entrance and elbow.

Manufactured elbow is shown in Figure 6.5; as seen in this figure, an apparatus has been used to connect this elbow to air pipes.

Figure 6.5 : Elbow.

Jet exit was designed as 90 degrees gap, which caused in a large pressure drop; so it has been changed to a 45 degrees gap as shown in Figure 6.6.

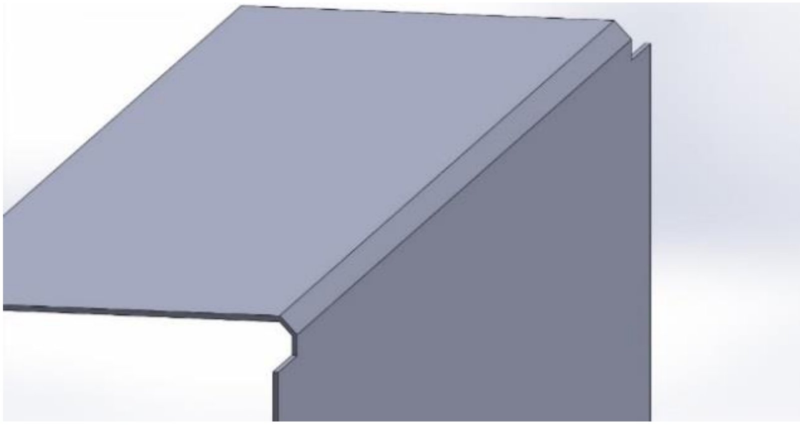

Figure 6.6 : Jet exit.

Front plate manufactured shape is shown in Figure 6.7.

Figure 6.7 : Front plate.

Top plate accompanied by its rear bended part is shown in Figure 6.8.

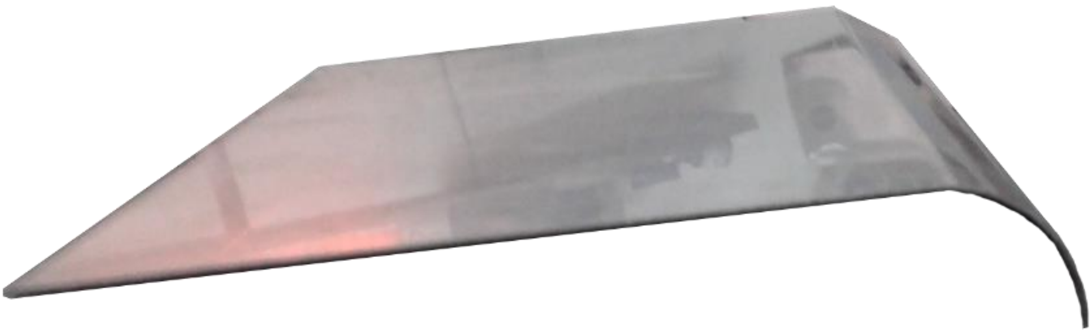

Figure 6.8 : Top plate with its rear bended part.

Figure 6.9 and Figure 6.10 show internal part of drawer in side and rear view; two other figures (Figure 6.11 and Figure 6.12) show internal part accompanied by the frame.

Finally, Figure 6.13 shows the apparatus which will be used to separate provided air by fan for two drawers.

Figure 6.9 : Internal parts manufactured shape in side view.

Figure 6.10 : Internal part manufactured state in rear view.

Figure 6.11 : The frame.

Figure 6.12 : Internal part attached to the frame.

Figure 6.13 : Air separation part.

Drawers' final condition is shown in Figure 6.14 and Figure 6.15.

Figure 6.14 : Drawer final manufactured condition.

Figure 6.15 : Drawer final manufactured condition.

7. SUGGESTIONS AND CONCLUSION

Different pneumatic fiber drawing systems have been probed; by doing a variety of CFD analysis, the most optimum design has been sought. In the sake of test, a cheap, easy to shape and light drawer has been manufactured using aluminum as material. It is determined that aluminum is deformed during the welding process and is not a suitable material in the sake of this project. Some hardships have been confronted in tightening process. Some experiments have been done using an available fan. The results of these experiments were that the fan capacity is not enough for this operation and internal design should be optimized aerodynamically. Supported with CFD analysis, the most aerodynamic design which causes in the least pressure drop has been detected. Stainless steel has been selected as the new drawer material and its manufacturing stage has been finished. Internal sections at final design have been selected in a condition which leads to the least possible pressure drop. To eliminate some hardships during the manufacturing stage, some slight changes have been done on chosen design.

It is obvious that designing a driver which includes narrowing air channels will cause in lowest pressure drop. Also, by getting nearer to jet, pressure drop increases; to decrease pressure drop at jet section, it should be designed in a state which has an angle of 45 degrees. Also, exploiting an air entrance which has as same diameter as fan exit will cause in the least pressure drop at primitive stages.

REFERENCES

[1] **A. Dahiya, M. G. Kamath, ve R. R. Hegde** (2004). Spunbond technology, *Retrieved May*, c 29, s 2008.

[2] **H. Lim** (2010). A Review of Spunbond Process, *J. Text. Appar. Technol. Manag.*, c 6, sayı 3.

[3] **Spunbond Technology.** (t.y.). Alındığı tarih: 20.02.2014, adres: ,http://www.engr.utk.edu/mse/Textiles/Spunbond%20Technology.htm

[4] **K. B. Subhash, B. Pourdeyhimi** (2012). Introduction to nonwovens technology, DEStech Publications, Inc.

[5] **US Patent 5292239** (t.y.). Apparatus for producing nonwoven fabric.

[6] **US Patent 3692618** (t.y.). Continuous Filament Nonwoven Web.

[7] **US Patent 6183684** (t.y.). Apparatus and method for producing non-woven webs with high filament velocity.

[8] **F. Lu, A. Moller** (1996). Advancing Spunbond Technology the Ultimate Way, *Nonwovens Conference*, TAPPI Proceedings, 51-56.

[9] **Baidurja, R., Rajesh, B., Lance, R.C.** (2014). Introduction to CFD Basics, Fluent Learning Module, ed: Lachance-Barret, S., United States.

CURRICULUM VITAE

Name Surname: Nasser Ghassembaglou

Place and Date of Birth: Iran- 21 September 1986

E-Mail: nasergasembagloo@gmail.com

EDUCATION:

B.Sc.: Mechanical Engineering- Heat and Fluids

M.Sc.: Mechanical Engineering- Mechanical Design

PROFESSIONAL EXPERIENCE:

2013-2015: ITU Mechanical Design Group, Researcher at TÜBİTAK project
2012-2013: ITU Fluids Group, Researcher at TÜBİTAK project
2009-2011: Azar Baharan Company, Supervisor and Technical Assistant.
June 2007-September 2007: Sewage and Water treatment center of East Azerbaijan, Internship.

REWARDS:

Full Scholarship on bachelor
Two Scholarships from TÜBİTAK during masters' education

SKILLS:

Solid Works
ANSYS- Fluent, ICEM-CFD and FSI
Auto-lisp and DCL Programming
Tecplot
Linux
C Programming
PHP Programming
HTML Programming

Adobe Flash
Adobe Dreamwaver
Adobe Photoshop
M.S. Office Programs

LANGUAGE SKILLS:

English- Fluent
Turkish- Fluent
Persian- Native
Azeri- Native
Arabic- Average

PUBLICATIONS, PRESENTATIONS AND PATENTS ON THE THESIS:

- **Nasser Ghassembaglou**, Abdullah Bolek, Oktay Yilmaz, Ertan Oznergiz, Hikmet Kocabas, Safak Yilmaz, 2015: Optimum Design of Attenuator of Spun-Bond Production System. *ICFDM 2015*, April 13-14, 2015 Venice, Italy.

OTHER PUBLICATIONS AND PRESENTATIONS:

- Mostafa Rahimi Dizaji, Aghil Yusefi-Koma, **Nasser Ghassembaglou** and Sina Shakoorzadeh, 2011: Wind Turbine Control with Fuzzy Supervisory in the Partial Load Region. *ICMEA conference at Thailand*, published in Advanced Materials Research Journal, July 31, 2011 Thailand.

- **Nasser Ghassembaglou**, Armin Rahmatfam, S.Faramarz Ranjbar, 2014: Optimum design of heat exchanger in diesel engine cold EGR for pollutants reduction. *ICAME 2014*, November 21-22, 2014 Paris, France.

- Leila Torkaman, **Nasser Ghassembaglou**, 2015: Evaporative Air Coolers Optimization for Energy Consumption Reduction and Energy Efficiency Ratio Increment. *ICFDM 2015*, April 13-14, 2015 Venice, Italy.